energies

Review

Inorganic p-Type Semiconductors: Their Applications and Progress in Dye-Sensitized Solar Cells and Perovskite Solar Cells

Ming-Hsien Li [1], Jun-Ho Yum [2,*], Soo-Jin Moon [3] and Peter Chen [1]

1 Department of Photonics, National Cheng Kung University, Tainan 701, Taiwan; l7894108@gmail.com (M.-H.L.); petercyc@mail.ncku.edu.tw (P.C.)
2 Molecular Engineering of Optoelectronic Nanomaterials Lab, Institute of Chemical Sciences and Engineering, School of Basic Sciences, Swiss Federal Institute of Technology, Lausanne CH-1015, Switzerland
3 Photovoltaic-Center, Centre Suisse d'Electronique et Microtechnique, Jaquet-Droz 1, Neuchâtel CH-2002, Switzerland; soo-jin.moon@csem.ch
* Correspondence: junho.yum70@gmail.com; Tel.: +41-21-693-3827

Academic Editor: Claudia Barolo
Received: 21 March 2016; Accepted: 25 April 2016; Published: 30 April 2016

Abstract: Considering the increasing global demand for energy and the harmful ecological impact of conventional energy sources, it is obvious that development of clean and renewable energy is a necessity. Since the Sun is our only external energy source, harnessing its energy, which is clean, non-hazardous and infinite, satisfies the main objectives of all alternative energy strategies. With attractive features, *i.e.*, good performance, low-cost potential, simple processibility, a wide range of applications from portable power generation to power-windows, photoelectrochemical solar cells like dye-sensitized solar cells (DSCs) represent one of the promising methods for future large-scale power production directly from sunlight. While the sensitization of n-type semiconductors (n-SC) has been intensively studied, the use of p-type semiconductor (p-SC), e.g., the sensitization of wide bandgap p-SC and hole transport materials with p-SC have also been attracting great attention. Recently, it has been proved that the p-type inorganic semiconductor as a charge selective material or a charge transport material in organometallic lead halide perovskite solar cells (PSCs) shows a significant impact on solar cell performance. Therefore the study of p-type semiconductors is important to rationally design efficient DSCs and PSCs. In this review, recent published works on p-type DSCs and PSCs incorporated with an inorganic p-type semiconductor and our perspectives on this topic are discussed.

Keywords: p-type semiconductor; inorganic material; dye-sensitized solar cell; perovskite solar cell; charge selective material; charge transport material

1. Introduction

Since the seminal paper of O'Regan and Grätzel in 1991 [1] dye-sensitized solar cells (DSCs) have become attractive for harvesting solar energy [2–6]. Recent developments have reported power conversion efficiencies (PCEs, η) exceeding 12%, achieved via optimization with materials such as panchromatic dyes and redox couples exhibiting higher redox potentials [7–11]. In DSCs, the dye absorbs light to form an exciton, then the charge generation is performed at the semiconductor-dye interface, and the semiconductor and the electrolyte serve as the charge transporting material. The typical DSC architecture based on a redox electrolyte is broadly composed five components: (1) a mechanical support coated with a transparent conductive oxide (TCO); (2) the semiconductor film, usually TiO_2; (3) a sensitizer (S) adsorbed on the surface of the semiconductor; (4) an electrolyte containing a redox mediator (M/M^-); (5) a counter electrode capable of regenerating the redox mediator.

The sensitizer S is excited by absorption of a photon (Equation (1)). Then the excited sensitizer S^* injects an electron into the conduction band of the semiconductor (Equation (2)). The injected electron flows through the n-SC network to the back contact and then through the external load to the counter electrode where it reduces the redox mediator (Equation (3)), which in turn regenerates the oxidized sensitizer S^+ (Equation (4)). This completes the circuit. Under illumination, the device constitutes a regenerative and stable photovoltaic energy conversion system. The overall efficiency of the device depends on optimization and compatibility of each of the constituents. Losses occur mainly through the recombination of the injected electrons either with the oxidized sensitizer (Equation (5)) or with the oxidized redox couple (M) at the n-SC surface (Equation (6)):

$$S_{(adsorbed)} + h\nu \rightarrow S^*_{(adsorbed)} \tag{1}$$

$$S^*_{(adsorbed)} \rightarrow S^+_{(adsorbed)} + e^-_{(injected)} \tag{2}$$

$$M + e^-_{(CE)} \rightarrow M^-_{(CE)} \tag{3}$$

$$S^+_{(adsorbed)} + M^- \rightarrow S_{(adsorbed)} + M \tag{4}$$

$$S^+_{(adsorbed)} + e^-_{(injected)} \rightarrow S_{(adsorbed)} \tag{5}$$

$$M + e^-_{(injected)} \rightarrow M^- \tag{6}$$

A solid-state hole transport material (HTM) has been widely used to replace the liquid electrolyte in DSC, which is to say that a hole transports through a p-SC as shown in Figure 1a. It is noteworthy that replacement of a solid-state HTM aims to avoid concerns about solvent leakage and corrosion from the typical iodide/triiodide redox couple in liquid electrolyte based DSC. The operating principle complies with the n-type sensitization. Therefore the sensitizer S is excited by absorption of a photon (Equation (1)). Then the excited sensitizer S^* injects an electron into the conduction band of the n-SC while the hole transports through HTM and arrives at the metallic cathode. 2,2′,7,7′-Tetrakis(*N*,*N*-di-*p*-methoxyphenylamine)-9,9′-spirobifluorene (spiro-OMeTAD) has been the most successful p-type organic conductor employed. Its work function is about 4.9 eV and the hole mobility, 10^{-4} $cm^2/(V\cdot s)$ [12]. Reported first in 1998 [13], the conversion yields have increased over the last decades, *i.e.*, from a fraction of a percentage to over 7% [14–19]. The origin of its good efficiency comes from the inherent properties of spiro-OMeTAD: amorphous, soluble, and small molecular size. However, its high cost, low hole mobility and lack of long term stability call for replacement with new hole transport materials including inorganic materials, e.g., NiO, CuI, CuSCN, $CsSnI_3$ and so on.

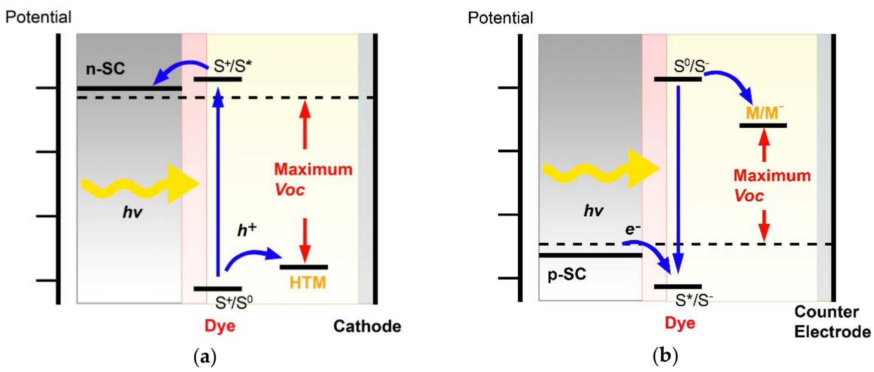

Figure 1. Schematic operating principle of (**a**) n-type solid-state dye-sensitized solar cell (SSDSC) and (**b**) p-type dye-sensitized solar cell (DSC) with a liquid electrolyte.

Most of the researches on DSCs have been devoted to architectures based on n-type semiconductors (n-SC) [20–24]. It is however possible to use a p-type semiconductor as photocathode.

The working principle is very similar to an n-type DSC, the difference being that the excited state of the sensitizer is now reductively quenched by the semiconductor, which is the sensitizer excited state injects holes into the valence band of the p-type semiconductor [25–27]. While the general design of dyes consists of electron-donor (D) and electron-acceptor (A) linked with π conjugation (D-π-A), the main difference between n-type dye and p-type dye is position of the acceptor: the anchoring group is attached on the electron-acceptor part for n-type dyes while the group is attached on the electron-donor part for p-type dyes. Under illumination, the sensitizer S is excited by absorption of a photon (Equation (1)) like n-type DSC. Then the excited sensitizer S^* injects a hole into the valence band of the semiconductor (Equation (7)). The injected hole flows through the semiconductor network to the back contact and then through the external load to the counter electrode where it oxidises the redox mediator (Equation (8)), which in turn regenerates the reduced sensitizer S^- (Equation (9), see Figure 1b):

$$S^*_{(adsorbed)} \rightarrow S^-_{(adsorbed)} + h^+_{(injected)} \tag{7}$$

$$M^- + h^+_{(CE)} \rightarrow M_{(CE)} \tag{8}$$

$$S^-_{(adsorbed)} + M \rightarrow S_{(adsorbed)} + M^- \tag{9}$$

The emerging solid-state organometallic lead halide perovskites have recently attracted tremendous attention because of their promising power conversion efficiencies which have been boosted to over 20% in recent years [28]. As evolved from solid-state DSCs, the common perovskite solar cells (PSCs) display device architecture that is composed of a compact titania dioxide layer, a mesoporous metal oxide scaffold infiltrated by the perovskite and covered by a perovskite capping layer, and a p-type organic semiconductor film contacted by silver or gold. Since the first successful application of spiro-OMeTAD in solid-state perovskite solar cells, spiro-OMeTAD has been extensively employed for fabrication of high-efficiency perovskite solar cells [29]. Recently, many HTMs have been demonstrated to replace spiro-OMeTAD aiming for low-cost and stability. The p-type contact materials for PSCs can be categorized into organic and inorganic semiconductors [30,31]. Organic HTMs, including small molecular and polymeric HTMs, are low-cost alternatives capable of low-temperature device processing. Small molecular HTMs are easy to purify, suitable for forming crystalline thin films, and feasible to match the band gaps of various perovskites by modifying their structures. On the other hand, polymeric HTMs present good stability and processibility, and are applied to fabricate PSCs with decent efficiency. The most widely used organic HTM, poly(3,4-ethylenedioxythiophene):poly(styrene sulfonate) (PEDOT:PSS), for the inverted p-i-n planar heterojunction perovskite solar cells has been reported to achieve a recorded PCE of 18.1% [32]. However, PEDOT:PSS causes device degradation due to its acidity and hydrophilic properties. Compared with organic HTMs, inorganic p-type semiconductors (*i.e.*, NiO, CuI, CuSCN, CuO and Cu_2O) as HTMs appear to be an ideal choice due to their low cost, ease of synthesis, high mobility, high transparency in the visible region and good chemical stability. Accordingly, PSCs employing inorganic HTMs have been demonstrated to exhibit decent stability. Furthermore, the use of inorganic charge transport layer of electron transport material (ETM) and HTM for PSCs has recently been demonstrated to protect the perovskite photoactive layer from exposure to ambient environments, thus enhancing the resistance to degradation of perovskite and achieving highly stable perovskite-based solar cells [33–36]. The scope of this perspective review is to present the recent developments in DSCs and PSCs based on inorganic p-type semiconductors, including NiO, CuSCN, CuI, Cu_2O and CuO.

2. p-Type Hole Transport Materials for DSCs

An appropriate HTM in solid-state dye-sensitized solar cells (SSDSCs) must satisfy several requirements: (i) the upper edge of the valence band of the p-type semiconductors must be located above the highest occupied molecular orbital (HOMO) ground state level of the dye; (ii) its hole mobility should be sufficiently high; (iii) it must be able to fill pores of mesoporous n-SC; (iv) it should be transparent in the range of dye absorption mostly, e.g., the visible light; and (iv) it should be stable during operation [13,37–41]. Copper-based inorganic semiconducting hole transport materials, such as CuI, CuSCN, CuO and Cu_2O, have shown promises for their use in dye-sensitized and quantum dot-sensitized solar cells. These materials can be deposited with solution process with good pore-filling. Meanwhile, these wide-band-gap semiconductors have high conductivity, suitable energy level and good transparency.

2.1. CuSCN

Copper thiocyanate (CuSCN) serves as a universal hole-transport interlayer material for numerous optoelectronic applications, including transparent thin-film transistors, organic, dye-sensitized, and perovskite solar cells, and organic light-emitting diodes. CuSCN combines intrinsic hole-transport (p-type) characteristics with a large bandgap (>3.5 eV) to show good optical transparency throughout the visible to near infrared spectrum and is chemically robust owing to its polymeric structure [42,43]. CuSCN is readily available from commercial sources while it is inexpensive and fabricated by a variety of methods such as dip-coating, and spray-coating or doctor-blading, chemical bath deposition, and electrochemical deposition. Furthermore, deposition of CuSCN using low-temperature with solution processes makes it compatible with flexible substrates. As compared to the widely utilized HTM spiro-OMeTAD, CuSCN exhibits a superior optical transparency, higher hole mobility (0.01–0.1 $cm^2/(V \cdot s)$ *vs.* Spiro-OMeTAD: 1.6×10^{-3} $cm^2/(V \cdot s)$) and good chemical stability [44].

In 1996, O'Regan and Schwartz demonstrated SSDSC based on formed by a heterojunction with rhodamine-coated TiO_2 and electrodeposited CuSCN (TiO_2/dye/CuSCN), exhibiting an incident photon to current conversion efficiency (IPCE) of 2.2% (absorbed photon to current conversion efficiency (APCE) of >70%) [45]. Apparently improved photocurrent was demonstrated by Kumara *et al.* wherein CuSCN dissolved in *n*-propyl sulfide was deposited on Ru-dye coated TiO_2 film, showing PCE of 1.25% and J_{sc} of 3.52 mA/cm^2 [46]. In 2002, O'Regan *et al.* reported a further improved SSDSC by pore filling control, performing an efficiency of 2.1% with a higher photocurrent of ~8 mA/cm^2 [47]. The results so far, however, are far from comparable with liquid electrolyte-based DSCs because the recombination of electrons injected to n-SC with the S^+ or with CuSCN is relatively faster than that of liquid electrolyte-based DSCs [48]. Surface passivation of n-SC was introduced, e.g., Al_2O_3 on TiO_2 (2.1% with improved V_{oc}) [49] and MgO on SnO_2 (2.82% with 10.18 mA/cm^2) [50]. Conductivity enhancement was also addressed as another approach to further improve SSDSCs. Perera *et al.* demonstrated that an excess of SCN-doped CuSCN improved its conductivity via creation of acceptor levels located 0.9 eV above the valence band edge, resulting in an improved PCE of 2.39% from 0.75% [51]. In the same sense, modifications of the CuSCN crystal structure by introducing triethylamine-coordinated Cu(I) [52] or Cu(II) [53] were demonstrated. It was found that the triethylamine-coordinated Cu(II) led to hole conductivity from 0.01 to 1.42 S/m and its application into SSDSC achieved a PCE of 3.4% [53].

2.2. CuI

Another p-type wide-bandgap (~3.1 eV) semiconductor, copper iodide (CuI), is an ionic solid and serves as a potential candidate of HTM on the basis of its suitable valance band (VB) position, good optical transparency, higher hole mobility (0.5–2 $cm^2/(V \cdot s)$) over CuSCN, and compatibility of solution-deposited process with the perovskite absorber. In 1995, Tennakone *et al.* first demonstrated an SSDSC based on CuI HTM in conjunction with cyanidin dye [54], which was later improved by replacement with a Ru-bipyridyl complex dye, showing a PCE of 4.5% [55]. There have been several strategies for photovoltaic performance enhancement. For instance, retarding crystallization of CuI that is known to inhibit the pore filling of mesoporous n-SC was proposed to improve pore filling by addition of a small amount of 1-methyl-3-ethylimidazoliumthiocyanate (MEISCN) [56,57] or triethylamine hydrothiocyanate (THT) [58]. The resulting efficiency of 3.75% with impressive stability for about 2 weeks under continuous illumination was demonstrated [58]. Surface passivation with a thin MgO layer on mesoporous TiO_2 was applied [59,60] and its combination with THT treatment achieved an enhanced PCE of 4.7% [60]. Further improvement achieved by interfacial engineering to improve contact between CuI and dye molecules was demonstrated: [55,61–63] and the best PCE of 7.4% from SSDSC employing PEDOT:PSS modified with guanidine thiocyanate was reported by Sakamoto *et al.* in 2012 [64].

2.3. $CsSnI_3$

$CsSnI_3$ belongs to a class of semiconducting perovskites of the composition $CsSnX_3$ (X = Cl, Br, I or mixed halides) and exist in two polymorphs at room temperature: a yellow coloured one-dimensional double-chain structure (γ-$CsSnI_3$) and a black coloured three-dimensional perovskite structure (B-γ-$CsSnI_3$). Recently the B-γ-$CsSnI_3$ showed its potential as a HTM in SSDSC on account of its properties including a high hole mobility of 585 $cm^2/(V \cdot s)$ at room temperature, high p-type metal-like conductivity (>200 S/cm^2), and the well-matched VB with the HOMO of Ru dye (N719) for efficient charge separation [65,66]. Chung *et al.* showed that by doping $CsSnI_3$ with 5% SnF_2 the efficiency could be further improved and combination with fluorine plasma treated TiO_2 electrode and a photonic crystal introduction achieved 8.51% with a shadow mask [65]. Very recently Lee *et al.* demonstrated Cs_2SnI_6 as a HTM, where Sn is in the 4^+ oxidation state, which is to say that it is more stable over $CsSnI_3$. The SSDSC with Ru dye (Z907) showed a PCE of 4.63% and the cell with mixture dyes and introducing a phonic crystal achieved a PCE of 7.8% (It is noted that use of a mask is not described) [67]. Achievement of the high efficiencies has proved the potential of these materials and has opened up the opportunity to further optimize SSDSCs. We summarize the performance of p-type inorganic SC-based SSDSCs with their photovoltaic parameters in Table 1.

3. p-Type Sensitization for DSCs

Candidates for p-type semiconductors for sensitization must satisfy several fundamental parameters. The position of the valence band should be higher than the HOMO of the dye for effective hole injection from the photoexcited dye while the position should be favourably low enough to render high photovoltage, which is determined with the energy gap between the valence band and the redox potential of an electrolyte. On the other hand, the conduction band should be high enough to block electron injection from the photoexcited dye. Therefore wide-band gap p-type semiconductors such as nickel oxide (NiO, a band gap of ~3.6 eV) that are also resistant to photocorrosion are promising candidates. The surface of the semiconductor must exhibit high chemical affinity to an anchoring group of dye in order to promote the adsorption of the dyes on the surface. Mesoporous films that exhibit large surface area to accommodate high numbers of dyes, leading to high light harvesting efficiency must be easily formed in a cost effective way. The molecular dye films adsorbed on a flat surface can only harvest a negligibly small fraction of the incoming light. Indeed, monolayers of porphyrins, which have among the highest extinction coefficients known, absorb far less than 1% of the sun sepctrum, derived from the Equation (10):

$$LHE\,(\lambda) = 1 - 10^{-A} = 1 - 10^{-\sigma\Gamma} \tag{10}$$

where A is the absorption optical density of sensitized film, $\sigma$is the absorption cross section (cm^2/mol) which equals to the product of ε (the molar extinction coefficient $M^{-1} \cdot cm^{-1}$) and 1000 (cm^3/L), Γ is the dye loading per projected surface area of the film. For a 10 µm-thick film the surface is enlarged over 1000 times allowing for efficient harvesting of sunlight, so high surface area materials needs to increase the light harvesting efficiency (LHE) of a sensitizer layer as a consequence of high number. In this respect, nano-scale materials, e.g., nanoparticles, nanorods, nanowires *etc.* have been demonstrated as a good candidate.

3.1. NiO

Since He *et al.* first demonstrated the generation of a cathodic photocurrent from organic dye sensitized nanostructured NiO cathode [68], many sophisticatedly designed dyes have been reported (details about their molecular structures can be found in [26]). Among them, a donor-acceptor type dye, comprising a perylene monoimide (PMI) as the acceptor and an oligothiophene coupled to triphenylamine as the donor holds the record efficiency of 0.41% [27]. The use of the tailored bridge lengths allowed for the control over the charge recombination events and the charge recombination was decelerated by several orders of magnitude [27]. A main drawback of NiO is the hole diffusion coefficient in the range of 10^{-8} to10^{-7} cm^2/s [69,70], which is several orders of magnitude lower than the electron diffusion coefficient in TiO_2. Therefore, intriguing routes to form good quality NiO films have been reported [70–77]. Sumikura *et al.* demonstrated good quality NiO electrodes obtained by the use of poly(ethylene oxide)-poly(propylene oxide)-poly(ethylene oxide) triblock copolymers as a template [72] and Li *et al.* demonstrated a PCE of 0.15% with a modified method [70], combined with a p-type dye, P1 (the triphenylamine moiety as the electron donor, malononitrile moiety as the electron acceptor, and a thiophene unit as the conjugated chain) [71]. Nanostructured NiO microballs (μBs) were synthesized by a thermolysis method and applied in p-DSCs. The high surface area and favourable pore size distribution of NiO-μBs facilitate increasing dye loading, leading to high J_{sc} (7.0 mA/cm^2) and IPCE (74%) with a PCE of 0.46% [74]. Electrode films composed of one-dimensional structures are expected to offer improved charge transport over a random polycrystalline network [78]. Crystalline NiO nanorods (NR) with average diameters of sub-10 nm formed through a nanocasting process, using mesoporous SiO_2 as a template was reported and its application in p-DSC achieved a PCE of 0.40% with improved V_{oc} (292 mV) and fill factor (*FF*) (41%) [75]. Another interesting result reported by Gibson *et al.* was demonstration of a scalable method for the preparation of nanoporous NiO electrodes. A film composed of NiO nanoparticles formed by spraying method was sintered using a technique based on microwave-assisted plasma sintering (called rapid discharge sintering, RDS), which was faster than the conventional sintering process. Its application in P1-sensitized p-type DSC achieved overall efficiencies as high as 0.12% and IPCEs of about 50% [76]. Very recently, Zhang *et al.* demonstrated a solid state p-type DSC in which NiO is employed as a p-SC, and the triphenylamine (TPA) based organic dye P1 as a sensitizer, and a solid electron transport material (ETM), phenyl-C61-butyric acid methyl ester (PCBM), is employed to replace liquid redox couple electrolyte [79]. Although the p-SSDSC device gave a low J_{sc} of 50 $\mu A/cm^2$, a promising V_{oc} of 620 mV was demonstrated and that an electron transfer to PCBM and a hole injection into NiO from the excited dye was proved by ultrafast transient absorption spectroscopy.

3.2. Cu(I) Delafossite

The valence band of NiO as low as +0.5 V *vs.* NHE limits the photovoltage from p-DSCs and other type p-SC like CuSCN- [80,81], CuO- [82], GaP- [83], and Cu(I)-based delafossites have been proposed as an alternative. Among them, the Cu(I)-based delafossite materials ($CuMO_2$, M = Cr, Ga, Al) have shown promising results because of their deeper position of the valence band edge and optical transparency in the visible range. Moreover, in Cu(I)-based delafossite materials, that Cu 3d orbitals strongly hybridize with the O 2p orbitals, making the hole charge carriers be delocalized both on oxygen and copper atoms [84] which facilitates the hole mobility, for instance 10–10^{-2} $cm^2/(V\cdot s)$ for $CuAlO_2$ and $CuGaO_2$ [84–86]. A solid-state reaction synthesized $CuAlO_2$ and hydrothermally synthesized $CuGaO_2$ proved V_{oc}s of 333 mV [87] and 357 mV [88], with respectively the following dye and redox mediator couples: PMI-6T-TPA and I_3^-/I^-, and PMI-NDI and Co^{3+}/Co^{2+} (dtb-bpy). However, the limited film surface area resulted in small currents below 0.4 mA/cm^2. More effort to decrease the size of $CuAlO_2$ and $CuGaO_2$ improved the current to 0.954 mA/cm^2 [89] and 2.05 mA/cm^2 [90] and the hydrothermally synthesized $CuCrO_2$ nanocrystals with a high surface area of 87.9 m^2/g, combined with the use of 1-methy-1*H*-tetrazole-5-thiolate (T^-)/disulfide dimer (T_2) redox shuttle, P1, and CoS counter electrode showed 1.73 mA/cm^2 [91]. Recently metal doped Cu-based delafossite compounds have been reported to increase electrical conductivity [92] or change surface affinity to increase dye adsorption [93] or control crystal size [94]. Ursu *et al.* demonstrated relatively higher J_{sc} (0.093 mA/cm^2) with 5% Al-doped $CuGaO_2$ nanoparticles with N719 sensitizer compared to J_{sc}

(0.046 mA/cm^2) of the cells using undoped $CuGaO_2$ [92]. The same group reported also Fe-doped $CuGaO_2$ as a photocathode in p-type DSCs [93]. Fe-doped $CuGaO_2$ increased hydrophilicity and adsorptivity of sensitizer compared to pure $CuGaO_2$ by formation of Fe^{3+}-OH species on the surface. More hydrophilic Fe-doped $CuGaO_2$ films resulted in slightly increased J_{sc} from 0.046 mA/cm^2 to 0.056 mA/cm^2. Renaud *et al.* reported an improved performance from Mg-doped $CuGaO_2$, which is attributed to an increased surface obtained by addition of small amounts of Mg, and a higher V_{oc} of 305 mV with a higher J_{sc} of 0.415 mA/cm^2 was achieved [95]. Very recently, Ga-doped $CuCrO_2$ nanocrystalline synthesized by a hydrothermal method has achieved an improved J_{sc} of 1.56 mA/cm^2 [96]. We summarize the performance of p-type DSCs incorporating p-type inorganic SC with their photovoltaic parameters in Table 1.

Table 1. Summary of photovoltaic characteristics of dye-sensitized solar cells (DSCs) based on p-type inorganic solar cells (SCs).

Type [1]	Architecture [2]	V_{oc} (V)	J_{sc} (mA/cm^2)	*FF* (%)	η (%) [5]	*Ref.*
CuSCN						
HTM	FTO/mp-TiO_2/N3/CuSCN/graphite	0.616	3.52	0.576	1.25	[46]
HTM	FTO/cp-TiO_2/mp-TiO_2/N3/CuSCN/graphite	0.60	7.8	0.44	2.1	[47]
HTM	FTO/cp-TiO_2/mp-TiO_2/Al_2O_3/N3/CuSCN/graphite	0.69	5.1	0.59	2.1	[49]
HTM	FTO/cp-SnO_2/mp-SnO_2/MgO/D149/CuSCN/graphite	0.544	10.18	0.51	2.82	[50]
HTM	FTO/mp-TiO_2/N3/SCN doped CuSCN/graphite	0.512	9.09	0.514	2.39	[51]
HTM	FTO/mp-TiO_2/N719/THT + CuSCN/Pt	0.578	10.52	0.556	3.39	[53]
CuI						
HTM	FTO/cp-TiO_2/mp-TiO_2/ZnO/N3/MEISCN + CuI/Au	0.59	6.84	0.57	3.8	[57] [3]
HTM	FTO/cp-TiO_2/mp-TiO_2/MgO/N3/ CuI/Au	0.51	8.74	0.54	2.9	[59] [4]
HTM	FTO/ mp-TiO_2/MgO/N3/CuI/Au	0.62	13	0.58	4.7	[60]
HTM	FTO/cp-TiO_2/mp-TiO_2/N3/CuI/PEDOT:PSS (carbon black: 200 wt%)	0.739	14.5	0.69	7.4	[64]
$CsSnI_3$						
HTM	FTO/mp-TiO_2/N719/$CsSnI_3$/ZnO PC/Pt	0.723	15.9	0.739	8.51	[65]
Cs_2SnI_6						
HTM	FTO/cp-TiO_2/mp-TiO_2/Z907/Cs_2SnI_6/Pt	0.571	13.2	0.613	4.63	[67]
HTM	FTO/cp-TiO_2/mp-TiO_2/multi-dyes/Cs_2SnI_6/Pt with 3D PC	0.618	18.6	0.680	7.80	
NiO						
p-DSC	FTO/mp-NiO/dye 3/I_3^- & I^-/Pt	0.218	5.35	0.35	0.41	[27]
p-DSC	FTO/2 steps-NiO/P1/I_3^- & I^-/Pt	0.084	5.48	0.34	0.15	[70]
p-DSC	FTO/NiO-μBs/PMI-6T-TPA/I_3^- & I^-/Pt	0.208	6.36	0.34	0.46	[74]
p-DSC	FTO/NiO-NR/PMI-6T-TPA/I_3^- & I^-/Pt	0.292	3.30	0.41	0.40	[75]
p-DSC	FTO/RDS-NiO /P1/I_3^- & I^-/Pt	0.125	2.84	0.34	0.12	[76]
Cu(I) delafossite						
p-DSC	FTO/$CuAlO_2$/PMI-6T-TPA /I_3^- & I^-/Pt	0.333	0.33	0.40	0.041	[87]
p-DSC	FTO/$CuAlO_2$/O_2/I_3^- & I^-/Pt	0.103	0.954	0.375	0.037	[89]
p-DSC	FTO/$CuGaO_2$/P1/Co^{3+} & Co^{2+}/Pt	0.357	0.165	0.308	0.018	[88]
p-DSC	FTO/$CuGaO_2$/P1/T^- & T_2/CoS	0.199	2.05	0.445	0.182	[90]
p-DSC	FTO/$CuGaO_2$:1%Mg/PMI-NDI/ Co^{3+} & Co^{2+}/Pt	0.305	0.415	0.35	0.045	[95]
p-DSC	FTO/$CuCr_{0.9}Ga_{0.1}O_2$/P1/I_3^- & I^-/Pt	0.134	1.56	0.489	0.10	[96]

[1] In type, "p-DSC" indicates "p-type sensitization"; [2] "FTO" is " fluorine-doped tin oxide". "cp" and "mp" indicate "compact film" and "mesoporous film". PEDOT:PSS is poly(3,4-ethylenedioxythiophene):poly(styrene sulfonate). "PC" indicates "photonic crystal". "μBs", "NR", and "RDS" indicates "microballs", "nanorod", and "rapid discharge sintering", respectively; [3] The intensity of the incident light of 61 mW/cm^2 is used; [4] The intensity of the incident light of 83 mW/cm^2 is used; [5] power conversion efficiency (PCE, η) = $J_{sc} \times V_{oc} \times FF/I_0$, where J_{sc} is the short circuit current density; V_{oc} is the open circuit voltage; *FF* is fill factor, and I_0 is the intensity of the incident light.

3.3. Tandems DSC

The development of p-type DSCs opens possibilities for significant improvement of existing n-type DSCs by making tandem cells. In a tandem DSC, the cathode of conventional n-type DSC is replaced by a photocathode based on a p-type semiconductor, for example, based on NiO. The architecture is shown in Figure 2.

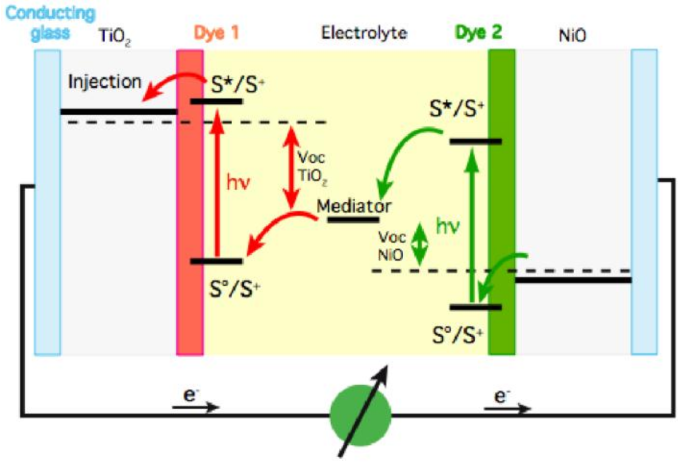

Figure 2. Operating principles of tandem dye-sensitized solar cells composed of n- and p-type semiconductors (taken from [97]).

The first promising advantage of the tandem DSC design is the obvious possibility to use two sensitizers with complementary spectral response, one on each type of semiconductor. The second advantage of such a design is the expected increase of the open circuit voltage. Indeed, in an n-type DSC, the maximum V_{oc} value, V_{oc}(n-SC) is considered to be the energy difference between the oxidation potential of the redox mediator and the energy level of the quasi-Fermi level in the n-type semiconductor. In a p-type DSC, the maximum V_{oc} value, V_{oc}(p-SC) is the energy difference between the oxidation potential of the redox mediator and the energy level of the quasi-Fermi level of the free electrons in the p-type semiconductor. In the tandem DSC, the maximum value for the open circuit voltage is the sum of both components, V_{oc} = V_{oc}(n-SC) + V_{oc}(p-SC). The proof of concept of this strategy has been reported in 2000, using N719 as a sensitizer on TiO_2 for the photoanode and erythrosine B as a sensitizer on NiO for the photocathode [98]. The performance of this system has been improved by more than 50% (from η = 0.39% to 0.66% under air mass (AM) 1.5) by using a mesoporous NiO film of higher quality [99].

Due to the definition of V_{oc} in a tandem DSC, it can be deduced that the electrochemical potential of the redox mediator has no impact on its value. Therefore it is possible to replace the I^-/I_3^- couple by the Co^{3+}/Co^{2+} (dtb-bpy) in the electrolyte without impacting the V_{oc} [25]. Finally, using a dye comprising triphenylamine-oligothiophene-PMI, a tandem DSC with a power conversion efficiency of 2.42% was obtained [27]. Taking into account that in this case, the spectral responses of both dyes were similar, this is a very promising result for future devices using dyes with a complementary spectral response.

4. p-Type Inorganic Hole Transport Materials for PSCs

In this section, we focus on recent developments in perovskite solar cells based on inorganic p-type semiconductors, including NiO, CuSCN, CuI, Cu_2O and CuO. Ideal HTMs for highly efficient PSCs are required to offer the following features: appropriate valence band for efficient electron blocking and hole collection, high hole mobility, stable thermal and optical properties. Based on the contact electrode polarity, DSC-like structures that work with n-i-p heterojunction are firstly introduced, followed by the organic photovoltaic (OPV)-like inverted structures of p-i-n heterojunction. With the evolution from mesoscopic sensitized junction, non-injecting super mesostructure scaffolds to planar perovskite solar cells, the configuration of photovoltaic devices can be categorized into mesoscopic and planar junction devices. For both DSC-like and OPV-like architecture, mesoscopic and planar PSCs schematically illustrated in Figure 3 are also reviewed.

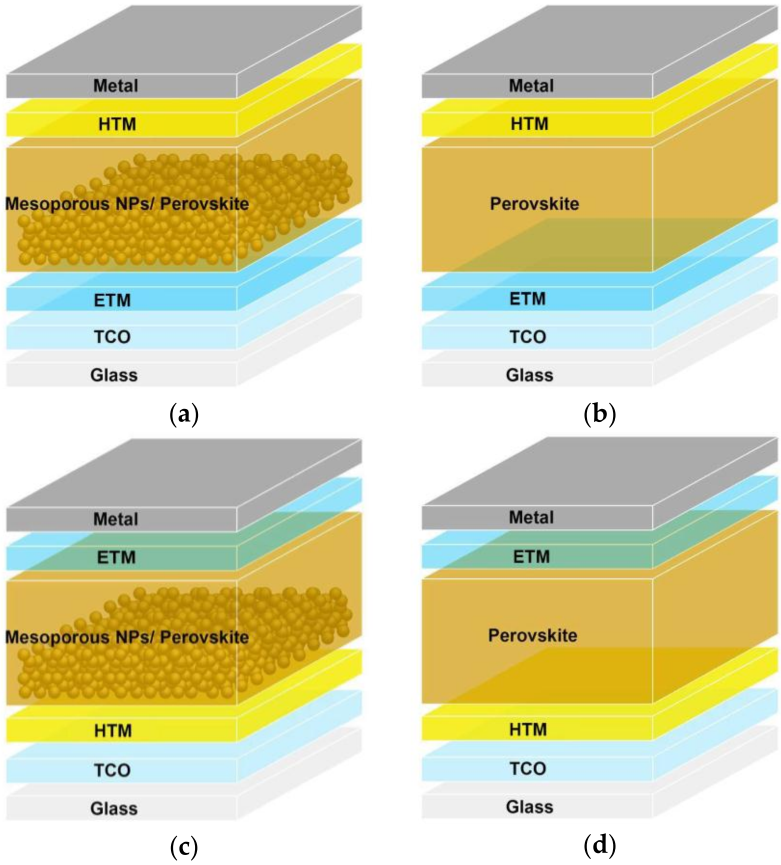

Figure 3. Schematic organometallic lead halide perovskite solar cell (PSC) architectures: (**a**) mesoporous n-i-p PSC; (**b**) planar n-i-p PSC; (**c**) mesoporous p-i-n PSC; and (**d**) planar p-i-n PSC.

4.1. NiO

As mentioned above, NiO is a low-cost material with superior properties, such as thermal and chemical stability, optical transparency, which has been demonstrated to be a good candidate of hole selective contact for PSCs in virtue of its suitable work function and suitable conduction band position to effectively transport holes and block electrons. In contrast to spiro-OMeTAD that requires multi-step organic synthesis and tedious purification, NiO can be prepared by simple and low-cost synthetic processes. A significant quenching of photo-luminescence emission from NiO/perovskite heterojunction confirms that NiO film effectively extracts holes from perovskite; though the first planar architecture of NiO/$CH_3NH_3PbI_{3-x}Cl_x$/PCBM obtained a low efficiency (<0.1%) mainly due to very poor perovskite coverage on the NiO surface [100]. Since then, many efforts have been devoted to improving the device efficiency using NiO as a hole transporter. The details are discussed in various device configurations.

4.1.1. Mesoporous NiO-Based n-i-p PSCs

Liu *et al.* introduced NiO nanoparticles to form a mesoporous NiO space separator between the mesoporous TiO_2 and the carbon counter electrode. A hetero p-n junction formed by NiO/TiO_2

junction easily separates electron and hole flow in opposite directions; hence, lower recombination could occur at this interface. The PSCs were composed of FTO/compact TiO_2/mesoporous TiO_2/mesoporous NiO/carbon, in which the light absorber $CH_3NH_3PbI_3$ was infiltrated inside the pores of mesoporous TiO_2/mesoporous NiO/carbon via sequential deposition [101]. Application of mesoporous NiO as a HTM effectively suppresses charge recombination and facilitates hole extraction, resulting in a cell with a PCE of 11.4% [102]. Furthermore, the same groups applied highly-crystalline NiO nanosheets as top nanostructured charge transport layers and inserted an additional mesoporous ZrO_2 layer to achieve an n-i-p heterojunction. The ZrO_2 layer was inserted to separate the mesoporous TiO_2 layer and the mesoporous NiO layer to suppress TiO_2/NiO interface charge recombination, leading to an enhancement of charge collection. A full device was fabricated as a structure of FTO/compact TiO_2/mesoporous TiO_2/mesoporous ZrO_2/mesoporous NiO/carbon/ sequentially deposited $CH_3NH_3PbI_3$, in which the mesoporous layers were prepared by a screen printing technique. The PSCs using all metal oxide semiconductors as a framework achieved a promising energy conversion efficiency of 14.2% [103]. Similar works were reported by Xu *et al.* who used a doctor-blade technique to fabricate mesoscopic TiO_2/ZrO_2/NiO/carbon structures that exhibited an appreciable PCE of 14.9% [104]. Under a similar configuration, a quadruple layer consisting of mesoscopic TiO_2/Al_2O_3/NiO/carbon was employed as a scaffold and deposited by screen-printing to fabricate mesoscopic PSCs. By optimizing the thickness of each layer, a considerable PCE of 15.03% was achieved for 800 nm-thick mesoporous NiO layer [105]. The above-mentioned mesoscopic devices displayed excellent stability due to the protection provided by the thick carbon counter electrode.

4.1.2. Planar NiO-Based n-i-p PSCs

Nejand *et al.* used a sputter-deposited NiO_x thin film on the perovskite light absorber to extract the generated holes from the perovskite layer. A nickel electrode was subsequently sputtered to replace the noble Au contact due to its vicinity of work function close to the valance band of perovskite. A planar n-i-p heterojunction PSC of FTO/compact TiO_2/$CH_3NH_3PbI_{3-x}Cl_x$/NiO_x/Ni was fabricated. The substrate was tilted 45° against the sputtering target for the formation of compact and uniform NiO_x layer covering on the perovskite surface. Also, periodic deposition by controlling the temperature was further employed to lower the substrate temperature without damaging the perovskite layer. The fabricated device initially displayed a low photovoltaic performance. After the strain release of the sputter-deposited NiO_x layer, high hole mobility in the NiO_x film was achieved and led to improve both V_{oc} and J_{sc}. Eventually, PSCs employing sputter-deposited NiO_x reached a maximum efficiency of 7.24% and impressive long-term durability of over 2 months. The results indicated that applications of inorganic ETM and HTM for PSCs would effectively hinder the water and oxygen penetration [36].

4.1.3. Mesoporous NiO-Based p-i-n PSCs

The original application of mesoporous NiO in PSCs was reported by Tian *et al.* [106] and our group nearly at the same time. Tian *et al.* fabricated mesoporous NiO-based PSCs with an architecture of FTO/compact NiO/mesoporous NiO/sequentially deposited $CH_3NH_3PbI_3$/PCBM/Al. After controlling the thickness of compact NiO film of 80 nm and that of mesoporous NiO layer of 120 nm, the best device exhibited an efficiency of 1.5% with extremely low FF and J_{sc} which is caused by high resistance at NiO/perovskite interface [106]. Our group incorporated a mesoporous NiO as a host to adsorb more amount of perovskite for the improvement of light harvesting [107]. A similar device structure was constructed as indium-doped tin oxide (ITO)/compact NiO/mesoporous NiO/sequentially deposited $CH_3NH_3PbI_3$/$PC_{61}BM$/bathocuproine (BCP)/Al. The energy level arrangement, in which the VB position of NiO is close to that of perovskite and the lowest unoccupied molecular orbital (LUMO) of $PC_{61}BM$ is nearly identical with the conduction band (CB) edge of perovskite, is suitable for receiving high output voltage and minimizing energy losses for the charge separation process between the absorber and selective contacts. The champion cell delivered a V_{oc} of

1.04 V, a J_{sc} of 13.24 mA/cm^2, and a *FF* of 69%, leading to an overall efficiency of 9.51%. Compared with our previously reported planar heterojunction junction (PHJ) device [108], the implementation of the mesoscopic NiO layer evidently ameliorates device performance for increased current response in the long wavelength part due to the improvement of light harvesting caused by a thicker perovskite layer. With elimination of a NiO compact layer, Zhu *et al.* employed an extremely thin mesoporous NiO layer as hole extraction and transport layer for efficient perovskite solar cell that was consisted of FTO/mesoporous NiO/sequentially deposited $CH_3NH_3PbI_3$/PCBM/Au. A corrugated surface resulted from aggregation of faceted NiO nanocrystals facilitated perovskite formation with good coverage and interconnectivity. By optimizing the thickness of the mesoporous NiO layer of 40 nm, its electron blocking ability was improved to reduce the charge recombination and leakage current. The best performance of NiO-based PSC displayed a V_{oc} of 0.882 V, a J_{sc} of 16.27 mA/cm^2, a *FF* of 0.635 and a PCE of 9.11% [109].

Furthermore, we introduced a low-temperature sputtered NiO_x film to serve as a pinhole-less compact layer for optimizing charge collection losses in the NiO/perovskite interface. A high quality NiO_x compact layer formed by sputter deposition has benefits in the charge collection, leading to a remarkable improvement in device performance and reproducibility as compared to the PSCs employing solution-processed NiO_x [107]. A full ITO/sputtered-compact NiO/mesoporous NiO/sequentially deposited $CH_3NH_3PbI_3$/PCBM/BCP/Al device was demonstrated, in which the compact NiO_x layer was deposited by RF magnetron sputtering system in pure Ar gas or a reactive sputtering method under a mixture of Ar and O_2 gas. By optimizing the oxygen doping ration of 10% and the thickness of mesoporous NiO layer, a decent PCE of 11.6% was obtained [110].

As revealed from the transient photo-induced absorption (PIA) spectrum, long-lived holes in the mesoporous NiO have been identified to prove the charge separation occurred at the NiO/perovskite interface. For efficient mesoporous NiO-based PSCs, it is critical to reduce the mesoporous NiO thickness and optimize the NiO/perovskite interface. In addition, replacement of non-injection scaffold is suggested to minimize the interface recombination [35]. Chen *et al.* reported the implementation of hybrid interfacial layer by incorporating an ultrathin NiO compact layer with a thin mesoporous Al_2O_3 scaffold to fabricate inverted PSCs with a FTO/compact NiO/mesoporous Al_2O_3/$CH_3NH_3PbI_3$/PCBM/BCP/Ag configuration [111]. The hybrid interfacial layer of NiO/mp-Al_2O_3 significantly minimizes light harvesting and interfacial recombination losses, in which thinner compact NiO layer and highly transparent mp-Al_2O_3 were utilized to prevent light absorption losses. Possible shunt paths between FTO and perovskite film are inhibited by introducing Al_2O_3 nanoparticles on the pinhole of NiO compact layer; in addition, mp-Al_2O_3 layer effectively blocks the shunt paths between NiO and PCBM. Devices using hybrid interfacial layer displayed a high *FF* of 0.72 with an acceptable PCE of 13.5%.

4.1.4. Planar NiO-Based p-i-n PSCs

For the demonstration of the first planar NiO-based perovskite solar cells, we employed a solution-processed NiO_x thin film as an electrode interlayer on the ITO substrate to realize $CH_3NH_3PbI_3$/PCBM PHJ hybrid solar cells. As evidence of effective PL quenching, NiO_x was expected to be a potential electrode for extracting hole carrier. To further overcome the coverage issue, a UV-ozone (UVO) treatment of the ITO/NiO_x substrate was performed to improve the surface wetting capability and resulted in an improvement of the perovskite coverage. The work function of NiO_x thin film was further modified to be 5.4 eV for better matching with the VB edge of $CH_3NH_3PbI_3$. The hybrid cell composed of ITO/spin-coated NiO_x/one-step deposited $CH_3NH_3PbI_3$/PCBM/BCP/Al was fabricated to deliver an efficiency of 7.8% [108]. Lai *et al.* proposed oxidized-Ni metal film with variant annealing temperature to realize NiO_x compact layer as a HTM. A full device with an ITO/compact NiO_x/one-step deposited $CH_3NH_3PbI_3$/PCBM/BCP/Al structure was fabricated. By oxidizing Ni metal with an annealing temperature of 450 °C, NiO_x film shows a smooth surface morphology that facilitates perovskite interconnectivity with pinhole-less surface coverage, leading to the best PCE of 7.75% [112]. The same group further employed Ni/Au bilayer to simultaneously function as HTM and conductive electrode by oxidizing this e-beam-sputtered film in O_2 atmosphere with annealing process. The bifunctional p-type electrode composed of proper thicknesses of Ni (10 nm) and Au (7 nm) under an annealing temperature of 500 °C shows acceptable optical transparent (transmission >60% in the visible spectrum), good electrical conductivity and favorable work function matching the VB of perovskite. A TCO-free PSC was fabricated with a device configuration of glass/Au:NiO_x/gas-assisted deposition $CH_3NH_3PbI_3/C_{60}$/BCP/Al, delivering a J_{sc} of 13.04 mA/cm^2, a V_{oc} of 1.02 V, a *FF* of 0.77 and a decent PCE of 10.24%. Improvements on V_{OC} and *FF* were attributed to the minimizing energy loss and superior electrical conductivity, as compared their last work [113]. Subbiah *et al.* used electrodeposited NiO and CuSCN films as HTMs for their FTO/HTM/$CH_3NH_3PbI_{3-x}Cl_x$/PCBM/Al device, in which the perovskite layer was deposited via coevaporation of $PbCl_2$ and CH_3NH_3I [114]. The results indicated that the NiO-based PSCs exhibit superior performance than the CuSCN-based PSCs because of lower series resistance and higher shunt resistance. The NiO-based device with UVO treatment displayed a J_{sc} of 14.2 mA/cm^2, a V_{oc} of 0.786 V, a *FF* of 0.65 and a PCE of 7.26% [115]. Hu *et al.* fabricated a solution-processed NiO compact layer by spin-coating a nickel acetate methoxy-ethanol solution. Similar structure of ITO/NiO/sequentially deposited $CH_3NH_3PbI_3$/PCBM/Al with UVO treatment was achieved to present device efficiency of 7.6% [116]. To further improve the quality of the NiO, Cui *et al.* exploited the reactive magnetron sputtering method to make a compact NiO film for a cell structure of FTO/sputtered NiO/solvent-engineering $CH_3NH_3PbI_3$/PCBM/BCP/Au. The solvent-engineering method was introduced to form a homogeneous surface coverage and uniform interlayer morphology of perovskite absorber onto the compact layer. With a 240 nm-thick perovskite and effective NiO electrode, the as-fabricated device exhibited an increased PCE of 9.84% [117].

On the whole, NiO-based PSCs generally exhibited a lower *FF* than the PEDOT-based devices although they displayed a higher V_{oc}. PSCs applying hybrid NiO_x/PEDOT HTM were further proposed by Park *et al.* to improve *FF*. With the addition of a PEDOT covering on a NiO_x-coated substrate, the NiO_x surface morphology was modified to be rough, which benefits increased interfaces of $NiO_x/CH_3NH_3PbI_3$ heterojunction and reduces interface resistance. A planar p-i-n PSC of ITO/hybrid NiO_x-PEDOT/$CH_3NH_3PbI_3$/PCBM/Ag with high conversion efficiency of 15.1% was presented by using PEDOT treatment of 1.0% (v/v). As proven by the PL spectra and impedance spectroscopy, the capability of PL quenching and interface charge transfer resistance (R_{CT}) at the NiO_x/perovskite interface significantly improved with the PEDOT treatment. The experimental results also exhibited neglected-hysteresis of the fabricated inverted PSC device [118]. Li *et al.* used an extremely thin NiO_x film of 10 nm as a hole extraction layer for a device composed of ITO/spin-coated NiO_x/ $CH_3NH_3PbI_3/C_{60}$/BCP/Ag. A high-quality perovskite layer was deposited by fast deposited crystallization [119] to form a compact surface coverage and flat interlayer morphology, and the NiO-based planar PSCs delivered a V_{oc} of 994 ± 15 mV, a J_{sc} of 20.4 ± 0.7 mA/cm^2, a *FF* of 0.669 ± 0.022 and a PCE of 13.6% ± 0.6%. It is surprising that a HTM-free PSCs was further demonstrated to exhibit superior performance compared to NiO_x-based PSCs. In the HTM-free PSCs, perovskite simultaneously functions as the light absorber and hole transporter [120]. With a UVO treatment of ITO substrate, the work function of ITO was improved to a higher value of 5.2 eV that reduced the energy barrier between ITO and perovskite layer. Moreover, UVO treatment effectively removes the residual organic species to lower surface energy, which benefits the deposition of perovskite layer. On the other hand, the perovskite layer deposited on the bare ITO substrate with a nano-sized rough surface morphology improved the perovskite/ITO heterojunction interface. Eventually, the HTM-free PSCs showed a higher J_{sc} of 21.7 ± 0.5 mA/cm^2, a higher *FF* of 0.718 ± 0.015 and a promising PCE of 15.0% ± 0.5% [121].

Recently, significant improvements on NiO-based PSCs were made by doping the NiO thin film or modifying the NiO/perovskite interface heterojunction [98–102]. Kim *et al.* demonstrated a high-efficiency planar PSC by using solution-processed copper (Cu)-doped NiO_x (Cu:NiO_x) as a

HTM [122]. With copper acetate doping in nickel acetate as precursor, a Cu-doped NiO_x was fabricated via the conventional sol-gel route with a sintering process at 500 °C to achieve high crystallinity. The device structure of ITO/Cu:NiO_x/$CH_3NH_3PbI_3$/$PC_{61}BM$/C_{60}/Ag was demonstrated with a high PCE of 15.4%, and the improvement was attributed to the enhanced electrical conductivity and charge extraction capability of Cu:NiO_x film, and favorable perovskite crystallization on Cu:NiO_x film. Moreover, the application of wider bandgap Br-doped perovskite solar absorber in Cu:NiO_x-based PSCs was further demonstrated to exhibit a high voltage output of 1.13 V and 1.16 V for $CH_3NH_3Pb(I_{0.8}Br_{0.2})_3$ and $CH_3NH_3Pb(I_{0.6}Br_{0.4})_3$ devices, respectively, because of less potential loss between work function of NiO_x and VB of Br-contained perovskite. In the following progress, the same group introduced low-temperature combustion process to fabricate Cu:NiO_x compact layer that was prepared by doping copper nitrate trihydrate into nickel nitrate hexahydrate and acetylacetone as a precursor. A highly crystalline Cu:NiO_x via combustion process at 150 °C exhibited similar work function of −5.3 eV compared to that of sol-gel processed Cu:NiO_x [98]. Moreover, combustion-processed Cu:NiO_x exhibited higher electrical conductivity than that of high-temperature-sintered film by almost two fold. PSCs fabricated with the configuration of ITO/Cu:NiO_x/$CH_3NH_3PbI_3$/C_{60}/bis-C_{60}/Ag displayed an recorded PCE of 17.74% [123]. Park *et al.* modified the NiO/perovskite interface heterojunction by employing the pulse laser deposition (PLD) method to fabricate a well-ordered nanostructured NiO thin film with a good optical transparency and preferred orientation of (111) [124]. The (111)-oriented NiO showed a lower resistivity and sheet resistance compared to other growth directions, which have the benefit of effectively extracting hole carriers and preventing recombination. Also, the well-ordered nanostructured NiO provides more contact interface with perovskite to slow the recombination rate during the charge collection. The full device was constructed as ITO/PLD-NiO/$CH_3NH_3PbI_3$/PCBM/LiF/Al with a dense perovskite prepared by a solvent engineering technique. By introducing a partial oxygen pressure of 200 mTorr and controlling the deposition time, a nanostructured NiO film with controlled thickness was made for high efficiency planar p-i-n heterojunction PSC. The best-performing device exhibited a J_{sc} of 20.2 mA/cm^2, a V_{oc} of 1.06 V and a remarkable efficiency of 17.3% with a very high *FF* of 0.813.

To further simplify the deposition procedure, Yin *et al.* employed solution-processed NiO_x film to fabricate an inverted planar PSC which was composed of FTO/NiO_x/$CH_3NH_3PbI_3$/PCBM/Ag [125]. The thickness of the NiO_x film significantly influences the photovoltaic performance, hysteresis effect and air storage stability of the as-fabricated devices. The thickness-dependent roughness would have impact on the charge collection. With the suitable thickness of 90 nm and nanostructure roughness of 3.835 nm for NiO_x compact layer, a hysteresis-free NiO_x-based PSC was fabricated with a PCE of 14.42%. Moreover, spin-coating NiO_x film via solution process was further applied to flexible PET substrate. Zhang *et al.* demonstrated flexible PSCs employing a room-temperature formation of NiO_x film to display an impressive PCE of 14.53% for the first time. A PET/ITO/NiO_x/$CH_3NH_3PbI_3$/C_{60}/bis-C_{60}/Ag structure was achieved, in which the formed NiO_x film is flawless with a nanostructure morphology feature that improves the hole extraction, and reduces the interfacial recombination and monomolecular Shockley-Read-Hall recombination of as-fabricated PSCs. Hysteresis-free with good air and mechanical stability of flexible NiO_x-based PSCs were thus achieved [126].

It is worth noting that the above-mentioned structures use PCBM as an ETM, whose stability and cost are issues of concern. Replacing organic charge extraction layers with inorganic materials would improve the devices' stability and provide versatile choices for material selection and device design. For the fabrication of durable and cost-effective PSCs, You *et al.* reported planar PSCs with all-solution-processed metal oxide charge transport layers, whose device structure consisted of ITO/NiO_x/$CH_3NH_3PbI_3$/ZnO/Al [33]. Favorable band alignment between the NiO_x film and perovskite material, and improved crystallinity of the perovskite film on NiO_x lead to cells with higher V_{OC} as compared to cells using PEDOT:PSS. On the other hand, ZnO film possesses strong hole-blocking effects originating from its deep VB, resulting in a higher J_{SC} for the ZnO-based PSCs. The all metal-oxide-based PSCs achieved a V_{oc} of 1.01 V, J_{sc} of 21.0 mA/cm^2 and *FF* of 76.0%, leading to a remarkable efficiency of 16.1%. With replacement of the aforementioned PCBM with ZnO, a significant enhancement in stability of un-encapsulated cells is achieved with a maintained PCE for 60 days under an ambient environment. By heavily doping metal oxide semiconductor as charge transport layer in planar PSCs, device performance of large active-area (>1 cm^2) with high-certified efficiency (>15%) and high stability under light soaking for 1000 h were further achieved [34]. Chen *et al.* employed heavily p-doped (p$^+$) $Ni_xMg_{1-x}O$ and n-doped (n$^+$) TiO_x as HTM and ETM, respectively, in inverted planar PSCs to improve charge transport capability and minimize resistive losses. As confirmed by transient photocurrent and photovoltage decay measurements, faster charge transport through the heavily-doped charge carrier extraction layers facilitate the charge extraction and prevent charge accumulation at the interface of HTM/$CH_3NH_3PbI_3$/ETM heterojunction. A remarkable efficiency of 18.3% is obtained with a very high FF of 0.83 for a small aperture area of 0.09 cm^2. So far, all high efficiency PSCs were measured for small areas of 0.1 cm^2; however, record efficiencies with cell sizes larger than 1 cm^2 are recommended by National Renewable Energy Laboratory (NREL) to compete with other solar devices. The PSCs employing highly-doped-metal-oxide charge extraction layers were fabricated with active area >1 cm^2, and the cell showed a considerable efficiency of 16.2%. Based on the inverted configuration, all metal-oxide-based PSCs display a small hysteresis with different scan directions. We summarize the NiO-based perovskite solar cells with their champion photovoltaic parameters in Table 2 and efficiency trends in Figure 4.

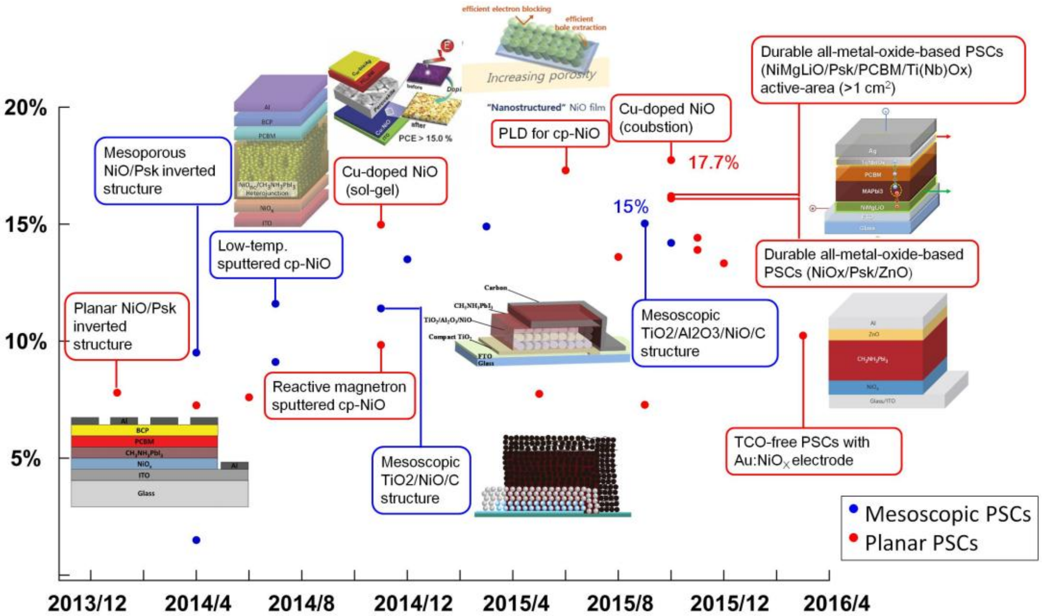

Figure 4. Power conversion efficiency (PCE) evolution of NiO-based organometallic lead halide perovskite solar cells (PSCs). C, carbon; cp, compact film; PLD, pulse laser deposition; Psk, perovskite; TCO, transparent conductive oxide.

4.2. CuSCN

As mentioned above, copper thiocyanate (CuSCN) serves as a universal hole-transport interlayer material for numerous optoelectronic applications because it has intrinsic hole-transport (p-type) characteristics with a large bandgap (>3.5 eV) and good optical transparency throughout the visible to near infrared spectrum. This material has been used both in n-i-p heterojunction and p-i-n heterojunction [91,103,104,106–109,111–113].

4.2.1. Meoporous CuSCN-Based n-i-p PSCs

CuSCN was first employed by Ito *et al.* into mesoporous PSC with a structure composed of FTO/compact TiO_2/mesoporous TiO_2/$CH_3NH_3PbI_3$/CuSCN/Au [127]. The $CH_3NH_3PbI_3$ light absorber was fabricated by one-step spin-coating [29] and its thickness is controlled by hot-air drying during spin-coating. With the introduction of doctor-blade processed CuSCN as a HTM and a controlled thickness of perovskite, the first CuSCN-based PSCs achieved a PCE of 4.85%. The experiment also indicates that the CuSCN films limit photovoltaic degradation of moisture-sensitive perovskite material. The same group further inserted Sb_2S_3 at the interface between mesoporous TiO_2 and perovskite layer to facilitate the crystallization of perovskite formation and serve as a passivation layer on TiO_2 to avoid decomposition of the perovskite crystals upon exposure to light [128]. The device showed a slight enhancement in performance to display a PCE of 5.12% and exhibited stability against light soaking without encapsulation. A remarkable improvement under the same configuration was further achieved by the sequential deposition method [129] and preheating substrate before PbI_2 deposition. The efficiency was enhanced to 10.51% because of a pinhole-less perovskite layer which limits the diffusion of CuSCN into the $CH_3NH_3PbI_3$ active layer [130]. The thickness of the perovskite film, perovskite capping layer, and surface morphology were further controlled with the sequential deposition method. It is noted that loading of PbI_2 upon the mesoporous TiO_2 was carried out by double spin-coating deposition for the purpose of perovskite capping layer formation. With the application of inorganic p-type HTM, CuSCN, made by doctor blading, the CuSCN-based solar cell displayed a promising performance with a J_{sc} of 19.7 mA/cm^2, a V_{oc} of 1.02 V, a *FF* of 0.62, and a PCE of 12.4% [131]. With addition of a small amount of methyl ammonium iodide (MAI) and DMSO in the PbI_2-DMF precursor, the light absorber of perovskite was made by the modified sequential two-step spin-coating method to form a pinhole-less film. A pinhole-less perovskite film effectively inhibited possible short contact between TiO_2 and CuSCN, resulting in enhancement on photovoltaic performance. A mesoporous PSC with the same structure of FTO/compact TiO_2/mesoporous TiO_2/$CH_3NH_3PbI_3$/CuSCN/Au displayed a V_{oc} of 0.96 V, a J_{sc} of 18.23 mA/cm^2, a *FF* of 0.68, and a PCE of 11.96%. A planar structure is fabricated for comparison to show a lower *FF* of 0.4, leading to a lower efficiency of 7.19% [132].

4.2.2. Planar CuSCN-Based n-i-p PSCs

For the implementation of CuSCN-based planar architecture, Chavhan *et al.* fabricated a solar cell composed of FTO/compact TiO_2/$CH_3NH_3PbI_{3-x}Cl_x$/CuSCN/Au. An organometal halide perovskite layer was deposited by spin-coating with a thermal annealing process [133]. The champion solar cell was exhibited for an annealing temperature of 110 °C because of a uniform perovskite morphology, leading to 6.4% power conversion efficiency. A lower V_{oc} of 727 mV was obtained and it was attributed to non-uniformity and poor surface coverage of $CH_3NH_3PbI_{3-x}Cl_x$ on the compact layer [134].

4.2.3. CuSCN-Based p-i-n PSCs

Subbiah *et al.* reported the use of CuSCN for planar OPV-like structures consisting of FTO/electrodeposited CuSCN/coevaporation $CH_3NH_3PbI_{3-x}Cl_x$/PCBM/Ag with a maximum efficiency of 3.8% [115]. When the perovskite film was deposited on the CuSCN film, a considerable PL quenching was observed to prove its effective charge extraction capability. However, without optimizing CuSCN film thickness, high series resistance and low shunt resistance result in poor photovoltaic performance for the CuSCN-based PSCs. Ye *et al.* used electrodeposited CuSCN film as HTM to fabricate inverted planar PSCs based on structure of ITO/CuSCN/$CH_3NH_3PbI_3$/C_{60}/BCP/Ag. By adopting a one-step fast deposition-crystallization (FDC) method [119], a high quality perovskite layer was formed on top of the CuSCN film. Lower interface resistance between the perovskite layer and CuSCN leads to pronounced improvements in J_{sc} and *FF* from 18.9 ± 1.9 mA/cm^2 to 21.7 ± 0.4 mA/cm^2 and 63.2% ± 4.4% to 74.2% ± 1.4%, respectively, as compared with the device prepared by two-step sequential deposition.

A significant increase of PCE was achieved from 11.0% ± 1.5% to 15.6% ± 0.6% [135]. To simplify the deposition procedure, a low-temperature processed CuSCN film was spin-coated onto the ITO substrate with nanocrystalline domains, followed by annealing at a low temperature of 100 °C. A planar inverted device of ITO/CuSCN/$CH_3NH_3PbI_3$/$PC_{61}BM$/bis-C_{60}/Ag was fabricated with a compact perovskite active layer deposited by the solvent engineering method. By optimizing the thickness of CuSCN of 40 nm, CuSCN-based PSCs achieved a promising efficiency of 16% and presented decent ambient stability. Interestingly, with further reduction of Ag thickness to 20 nm, a semitransparent PSC with an impressive efficiency of >10% was demonstrated [136]. Zhao *et al.* reported the similar device structure of ITO/spin-coated CuSCN/$CH_3NH_3PbI_3$/$PC_{60}BM$/LiF/Ag, in which the perovskite active layer was deposited by the solvent engineering method with a thickness of ~160 nm. A lower short current density of 15.76 ± 0.02 mA/cm^2 and fill factor of 63.2% ± 0.52% might be attributed to more abrupt perovskite crystalline interface and unsaturated thickness of absorber less than 300 nm, showing a lower PCE of 10.8% as compared with the previous CuSCN-based PSCs [137].

4.3. CuI

Christians *et al.* reported the first example by using CuI as a HTM in mesoscopic n-i-p PSCs with the best PCE of 6% [138]. The device configuration was constructed as FTO/compact TiO_2/mesoporous TiO_2/$CH_3NH_3PbI_3$/CuI/Au. Solution-deposited CuI was applied by an automated drop-casting method to form a 1.5 µm thick overlayer on top of the perovskite film. Though over-thick CuI exhibited a higher electrical conductivity than spiro-OMeTAD, CuI-based PSC exhibited a lower V_{oc} because of a high recombination rate as determined by impedance spectroscopy. Similarly, Sepalage *et al.* described the planar n-i-p PSCs with a structure of FTO/compact TiO_2/$CH_3NH_3PbI_3$/CuI/graphite. The planar perovskite layer was deposited using a gas-assisted spin-coating method [139] while the CuI layer and graphite layer were fabricated by doctor blading. Higher photovoltaic performance in V_{oc} was obtained compared to previously reported mesoscopic CuI-based devices, resulting in a higher efficiency of 7.5%. The superior voltage was caused by a reduced thickness of CuI film (~400 nm); however, it is still lower than the expected V_{oc} of ~1 V due to rapid recombination at the perovskite/CuI interface. On the other hand, the CuI-based devices displayed an apparent reduced *J-V* hysteresis under the DSC-like architecture. As regards steady-state current measurement, the CuI-based devices showed a faster response following voltage step. Rapid injection of holes from perovskite into the CuI layer prevents the capacitive current stored in the perovskite material and has positive contribution to diminish the *J-V* hysteresis [140].

Chen *et al.* employed solution-processed CuI as a HTM in inverted planar p-i-n PSCs with the architecture of FTO/CuI/$CH_3NH_3PbI_3$/PCBM/Al [141]. By using a vapor-assisted solution process to fabricate high quality perovskite light absorber [142], the device showed a promising performance with a V_{oc} of 1.04 V, a J_{sc} of 21.06 mA/cm^2, and a PCE of 13.58%. Benefiting from the high transmittance, nanostructure morphology and deep valance band of CuI thin film, CuI-based PSCs exhibit higher V_{oc} and J_{sc} than devices using PEDOT:PSS. Similarly, under the inverted architecture, CuI-based p-i-n PSCs showed a negligible hysteresis effect and acceptable ambient stability.

Table 2. Summary of photovoltaic characteristics of organometallic lead halide perovskite solar cell (PSC) based on inorganic hole transport material (HTM).

Type [1]	Architecture [2]	V_{oc} (V)	J_{sc} (mA/cm^2)	*FF* (%)	η (%) [3]	*Ref.*
NiO						
M	FTO/cp-TiO_2/mp-TiO_2/mp-NiO/Psk/carbon	0.89	18.2	0.71	11.4	[102]
M	FTO/cp-TiO_2/mp-TiO_2/mp-ZrO_2/mp-NiO/Psk/carbon	0.965	20.4	0.72	14.2	[103]
M	FTO/cp-TiO_2/mp-TiO_2/mp-ZrO_2/mp-NiO/Psk/carbon	0.917	21.36	0.76	14.9	[104]
M	FTO/cp-TiO_2/mp-TiO_2/mp-Al_2O_3/mp-NiO/Psk/carbon	0.915	21.62	0.76	15.03	[105]
M	FTO/cp-TiO_2/mp-TiO_2/mp-NiO/Psk/carbon	0.89	18.2	0.71	11.4	[102]
P	FTO/cp-TiO_2/Psk/NiO_x/Ni	0.77	17.88	0.53	7.28	[36]

Table 2. *Cont.*

Type [1]	Architecture [2]	V_{oc} (V)	J_{sc} (mA/cm^2)	FF (%)	η (%) [3]	Ref.
M	FTO/cp-NiO/mp-NiO/Psk/PCBM/Al	0.83	4.9	0.35	1.5	[106]
M	ITO/cp-NiO/mp-NiO/Psk/$PC_{61}BM$/BCP/Al	1.04	13.24	0.69	9.51	[107]
M	FTO/mp-NiO (sol-gel)/PsK/PCBM/Au	0.882	16.27	0.635	9.11	[109]
M	ITO/sputtered-NiO/mp-NiO/Psk/PCBM/BCP/Al	0.96	19.8	0.61	11.6	[110]
M	FTO/NiO/meso-Al_2O_3/Psk/PCBM/BCP/Ag	1.04	18.0	0.72	13.5	[111]
P	ITO/NiO_x/Psk/PCBM/BCP/Al	0.92	12.43	0.68	7.8	[108]
P	ITO/NiO_x (Ni-oxidized)/Psk/PCBM/BCP/Al	0.901	13.16	0.65	7.75	[112]
P	(TCO-free) Au:NiO_x/Psk/C_{60}/BCP/Al	1.02	13.04	0.77	10.24	[113]
P	FTO/NiO/Psk/PCBM/Al	0.786	14.2	0.65	7.26	[115]
P	ITO/NiO/Psk/PCBM/Al	1.05	15.4	0.48	7.6	[116]
P	FTO/sputtered-NiO/Psk/PCBM/BCP/Au	1.10	15.17	0.59	9.84	[117]
p	FTO/NiO_x/Psk/PCBM/Ag	1.09	17.93	0.74	14.42	[125]
P	ITO/Cu:NiO_x(sol-gel)/Psk/PC61BM/C60/Ag	1.11 ± 0.01	18.75 ± 0.42	0.72 ± 0.01	14.98 ± 0.33	[122]
P	ITO/Cu:NiO_x(combustion)/PsK/C60/bis-C60/Ag	1.05	22.23	0.76	17.74	[123]
P	ITO/PLD-NiO/Psk/PCBM/LiF/Al	1.06	20.2	0.813	17.3	[124]
P	PET/ITO/NiO_x/ Psk/C60/Bis-C60/Ag	0.97 ± 0.01	20.55 ± 0.71	0.68 ± 0.03	13.33 ± 0.78	[126]
P	ITO/hybrid NiO_x-PEDOT/Psk/PCBM/Ag	1.02 ± 0.006	19.4 ± 0.3	0.70 ± 0.016	13.9 ± 0.4	[118]
P	ITO/NiO_x/Psk/C_{60}/BCP/Ag	0.994 ± 0.015	20.4 ± 0.7	0.669 ± 0.022	13.6 ± 0.6	[121]
P	ITO/NiOx/Psk/ZnO/Al	1.01	21.0	0.76	16.1	[33]
P	FTO/NiMgLiO/Psk/PCBM/Ti(Nb)O_x/Ag (active area >1 cm^2)	1.072	20.21	0.748	16.2	[34]
CuSCN						
M	FTO/cp-TiO_2/mp-TiO_2/Psk/CuSCN/Au	0.63	14.5	0.53	4.85	[127]
M	FTO/cp-TiO_2/mp-TiO_2/Sb_2S_3/Psk/CuSCN/Au	0.57	17.23	0.52	5.12	[128]
M	FTO/cp-TiO_2/mp-TiO_2/Psk/CuSCN/Au	1.025	17.91	0.57	10.51	[130]
M	FTO/cp-TiO_2/mp-TiO_2/Psk/CuSCN/Au	1.016	19.7	0.62	12.4	[131]
M	FTO/cp-TiO_2/mp-TiO_2/Psk/CuSCN/Au	0.96	18.23	0.68	11.96	[132]
P	FTO/cp-TiO_2/Psk/CuSCN/Au	0.97	18.42	0.40	7.19	[132]
P	FTO/cp-TiO_2/Psk/CuSCN/Au	0.727	14.4	0.62	6.4	[133]
P	FTO/CuSCN/Psk/PCBM/Ag	0.677	8.8	0.63	3.8	[115]
P	ITO/CuSCN/Psk/C_{60}/BCP/Ag	0.97 ± 0.02	21.7 ± 0.4	0.742 ± 0.014	15.6 ± 0.6	[135]
P	ITO/CuSCN/Psk/$PC_{61}BM$/bis-C_{60}/Ag	1.07 ± 0.01	19.6 ± 0.3	0.74 ± 0.03	15.6	[136]
P	ITO/CuSCN/Psk/$PC_{61}BM$/bis-C_{60}/semitransparent Ag	1.06 ± 0.02	13.0 ± 0.4	0.73 ± 0.02	10.06	[136]
P	ITO/CuSCN/Psk/$PC_{60}BM$/LiF/Ag	1.06 ± 0.01	15.76 ± 0.02	0.632 ± 0.052	10.5 ± 0.16	[137]
CuI						
M	FTO/cp-TiO_2/mp-TiO_2/Psk/CuI/Au	0.55	17.8	0.62	6.0	[138]
P	FTO/TiO_2/Psk/CuI/graphite	0.78	16.7	0.57	7.5	[140]
P	FTO/CuI/Psk/PCBM/Al	1.04	21.06	0.62	13.58	[141]
Cu_2O						
P	(Simulation) FTO/TiO_2/Psk/Cu_2O/Au	1.2	24.75	0.82	24.4	[143]
P	ITO/Cu_2O/Psk/$PC_{61}BM$/Ca/Al	1.07	16.52	0.755	13.35	[144]
P	ITO/Cu_2O/Psk/PCBM/Al	0.89	16.52	0.58	8.30	[145]
P	(Simulation) FTO/Cu_2O/Psk/PCBM/Al	0.91	20.22	0.74	13.6	[146]
CuO						
P	ITO/CuO/Psk/$PC_{61}BM$/Ca/Al	1.06	15.82	0.725	12.16	[144]

[1] In type, "M" and "P" means "mesoporous" and "planar"; [2] "cp" and "mp" indicate "compact film" and "mesoporous film"; [3] PCE (η) = $J_{sc} \times V_{oc} \times FF/I_0$, where J_{sc} is the short circuit current density, V_{oc} is the open circuit voltage, FF is fill factor, and I_0 is the intensity of the incident light; BCP, bathocuproine; FTO, fluorine-doped tin oxide; ITO, indium-doped tin oxide; PCBM, phenyl-C61-butyric acid methyl ester; Psk, perovskite; TCO, transparent conductive oxide.

4.4. Cu_2O and CuO

Other well-known p-type semiconductors are Cu-based oxides such as cuprous oxide (Cu_2O) and copper oxide (CuO). They were recently applied as HTM for PSCs to minimize the energy loss because of their low-lying valence bands [119–122]. The n-i-p heterojunction planar PSC of glass/FTO/TiO_2/$CH_3NH_3PbI_3$/HTM/Au with NiO, CuI, CuSCN, Spiro-OMeTAD, and Cu_2O as HTM is simulated *via* a new solar cell simulation software, wxAMPS (the Analysis of Microelectronic and Photonic Structure). The optimized thickness of ETM and HTM are 135–145 nm and 350–450 nm, respectively, and that of the perovskite absorber layer is 350–450 nm. The PCE values with the various HTMs display a ranking of Cu_2O-, CuSCN-, Spiro-OMeTAD-, CuI-, and NiO-based PSC, among which the simulation of Cu_2O-based PSC exhibit the highest efficiency exceeding 24% [143]. The result indicates that it is possible to further increase the performance of PSCs by using copper oxide as HTM.

A planar inverted p-i-n heterojunction architecture of ITO/HTM/$CH_3NH_3PbI_3$/$PC_{61}BM$/Ca/Al was experimentally demonstrated by inserting Cu_2O or CuO as HTM. Cu_2O film was fabricated by converting the CuI-spin-coated substrate via aqueous NaOH solution while CuO film was formed by heating Cu_2O film in air [144]. With the addition of NH_4Cl dissolved in $CH_3NH_3PbI_3$ precursor, it has benefit of making uniform and high coverage perovskite light absorbers on the HTM; thus, more crystalline $CH_3NH_3PbI_3$ film was formed on Cu_2O and CuO films. The experimental results indicate that Cu_2O-based and CuO-based PSCs display enhanced V_{oc} of 1.07 and 1.06 V, respectively, and higher J_{sc} of 16.52 and 15.82 mA/cm^2, leading to the best PCE of 13.35% and 12.16%, respectively. As compared to the photovoltaic performance of PEDOT:PSS-based PSC (V_{oc} of 0.95 V, J_{sc} of 14.82 mA/cm^2 and PCE of 11.04%), enhanced V_{oc} resulted from the valance band of Cu_2O and CuO matching with that of the perovskite, and higher crystallinity of $CH_3NH_3PbI_3$ on Cu_2O and CuO improves the carrier transport to increase J_{sc} [144]. Chatterjee *et al.* prepared a high degree of crystallinity Cu_2O as a HTM through a successive ionic layer adsorption and reaction (SILAR) method. A similar device with a structure of ITO/Cu_2O/one-step deposited $CH_3NH_3PbI_3$/PCBM/Al was demonstrated with an efficiency of 8.23% [145]. Compared to the devices employing NiO or Cu:NiO HTM, Cu_2O-based PSCs exhibited a superior performance by virtue of the higher mobility of Cu_2O, low energy loss determined by scanning tunneling spectroscopy, low Cu_2O/perovskite interface recombination loss, and better perovskite crystallinity on Cu_2O film. Moreover, Wang *et al.* conducted a theoretical calculation on the Cu_2O/perovskite heterojunction solar cells by using the wxAMPS software. Models of inverted planar PSCs were performed with the configuration of FTO/HTM/$CH_3NH_3PbI_{3-x}Cl_x$/PCBM/Al, in which NiO_x and Cu_2O were applied as HTM, and the defect states are considered to take part in the interface recombination [116]. An efficiency of 9.88% was first simulated for NiO_x-based device to verify the experimental results with a thickness of 500 nm for the perovskite absorber layer. For high mobility Cu_2O with 10–50 nm thickness, PSCs using Cu_2O with 500 nm-thick perovskite absorber was further simulated to achieve a PCE of above 13% [146]. Photovoltaic parameters of CuSCN-, CuI, Cu_2O-, CuO-based perovskite solar cells are summarized in Table 2 and their efficiency trends are shown in Figure 5.

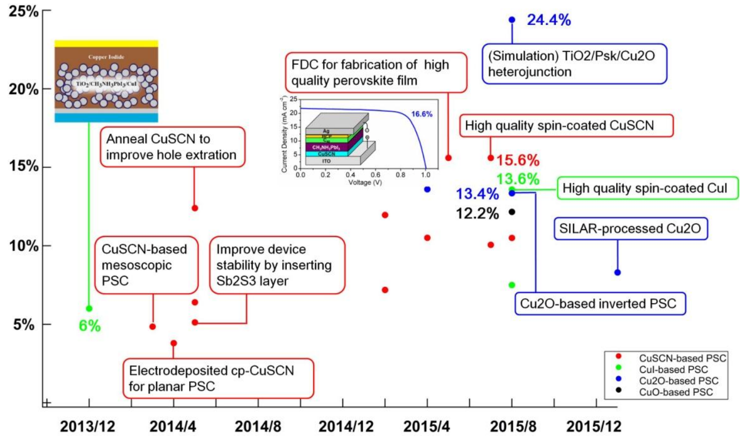

Figure 5. Power conversion efficiency (PCE) trends of CuSCN-, CuI, Cu_2O-, CuO-based organometallic lead halide perovskite solar cell (PSC). cp, compact film; FDC, fast deposition-crystallization; Psk, perovskite; SILAR, successive ionic layer adsorption and reaction.

5. Summary

The versatility of p-type inorganic semiconductors as a HTM, a semiconductor for p-type sensitization, a charge selective layer, *etc.* for solar cell applications is summarized. As for p-type DSC, the performance is not yet comparable to n-type DSCs. Probably alternatives with deeper VB than NiO as well as with high charge mobility and controlled size and morphology would improve the photovoltage. Not only that, material development of the other components, e.g., sensitizers and electrolytes, and their interfacial engineering in order to mitigate the charge recombination would be another strategy to improve overall performance. Further improvement of p-DSC will be one of keys to achieve high performance tandem solar cells. SSDSC based on p-type inorganic SC has shown a great improvement and the record efficiency of 8.5% obviously proves its potential over organic-based HTMs.

We also comprehensively surveyed the latest progress in PSCs using inorganic p-type semiconductor as HTMs. Briefly, good HTM candidates for efficient PSCs should have the following properties: (1) suitable valance band position to minimize the energy loss; (2) efficient charge transporting and blocking capability; and (3) high carrier mobility. As revealed, diverse inorganic p-type semiconductor having favorable VB, including NiO, CuSCN, CuI, Cu_2O and CuO, have been introduced to demonstrate efficient PSCs with enhanced device stability, among which Cu_2O is a promising candidate for highly efficient PSCs due to its superior hole mobility and deeper valance band. It is noted that choosing a HTM with high transparency throughout the visible and near infrared spectrum minimizes the optical loss for OPV-like architectures. Furthermore, proper control of surface energy will affect the crystallization kinetics and film quality of the perovskite film deposited on top of it. Combined with versatile fabrication processes for producing high quality uniform, dense and pinhole-free perovskite absorbers such as solvent engineering, fast deposition crystallization, vapor deposition, and additives, the device performance is apparently approaching the performance of conventional DSC-like PSC devices. The balance between charge separation, transportation and recombination shall be considered for optimizing the internal surface area and mesoscopic p-type oxide film thickness.

6. Future Trends

For future improvement of device performance, several issues deserve further investigations. For HTM in solid DSCs, pore-filling is one of the major challenges for inorganic p-type SCs. It is critical to form an intimate heterojunction inside the mesoscopic layer. For p-type sensitization DSCs, improving the crystal quality, increasing the energy offset from the potential of redox mediator, increasing the surface area, and inhibiting the interfacial recombination are critical areas. Novel p-type sensitizers are another main area to be explored to optimize energy level matching and charge transfer kinetics. Increasing open circuit voltage could be achieved by choosing oxides with deeper VB in combination with compatible dye HOMO. As for perovskite solar cells, increasing the mobility and conductivity in p-type oxide layer is important for receiving high efficiency PSCs. On the other hand, doping and optical absorption shall be carefully managed for achieve high overall performance. Except for the enhancement of photovoltaic performance, flexibility and long-term stability should be further addressed in the relevant issues. Low temperature procedure for ETM/HTM is required to offer the feasibility on the flexible substrate. $MAPbI_3$-based perovskite solar cells using solution-processed n-type/p-type metal oxide materials have shown great promises in facile fabrication and ambient stability. Other p-type materials such as spinel, Cu or Cr-based oxide may find their success in PSCs.

Acknowledgments: Peter Chen acknowledges the research grant from the Ministry of Science and Technology (MOST) of Taiwan under the grant-in-aids 103-2221-E-006-029-MY3 and 105-2623-E-006-002-ET.

Author Contributions: All authors contributed to this work from literature summary and writing to revision.

Conflicts of Interest: The authors declare no conflict of interest. The funding sponsors had no role in the design of the study; in the collection, analyses, or interpretation of data; in the writing of the manuscript, and in the decision to publish the results.

Abbreviations

The following abbreviations are used in this manuscript:

DSC	Dye-sensitized solar cell
n-SC	n-Type semiconductor
p-SC	p-Type semiconductor
PSC	Organometallic lead halide perovskite solarcell
TCO	Transparent conductive oxide
D	Electron-donor
A	Electron-acceptor
π	π Conjugation
S	Sensitizer
HTM	Hole transport material
ETM	Electron transport material
SSDSC	Solid-state dye-sensitized solar cells
HOMO	Highest occupied molecular orbital
LUMO	Lowest unoccupied molecular orbital
IPCE	Incident photon to current conversion efficiency
APCE	Absorbed photon to current conversion efficiency
VB	Valence band
CB	Conduction band
spiro-OMeTAD	2,2′,7,7′-Tetrakis(*N*,*N*-di-*p*-methoxyphenyamine)-9,9′-spirobifluorene
PEDOT	Poly(3,4-ethylenedioxythiophene)
PSS	Poly(styrene sulfonate)
V_{oc}	Open circuit voltage
J_{sc}	Short circuit current density
FF	Fill factor
PCE	Power conversion efficiency (= η)
FTO	Fluorine-doped tin oxide
ITO	Indium-doped tin oxide
MEISCN	1-Methyl-3-ethylimidazoliumthiocyanate
THT	Triethylamine hydrothiocyanate
LHE	Light harvesting efficiency
TPA	Triphenylamine
cp	Compact
mp	Mesoporous
dtb-bpy	di-*tert*-Butylbipyridine
P	Planar
Psk	Perovskite
BCP	Bathocuproine
PHJ	Planar heterojunction junction

References

1. O'Regan, B.; Grätzel, M. A low-cost, high-efficiency solar-cell based on dye-sensitized colloidal TiO_2 films. *Nature* **1991**, *353*, 737–740. [CrossRef]
2. Hagfeldt, A.; Grätzel, M. Light-induced redox reactions in nanocrystalline systems. *Chem. Rev.* **1995**, *95*, 49–68. [CrossRef]
3. Hagfeldt, A.; Grätzel, M. Molecular photovoltaics. *Acc. Chem. Res.* **2000**, *33*, 269–277. [CrossRef] [PubMed]
4. Grätzel, M. Photoelectrochemical cells. *Nature* **2001**, *414*, 338–344. [CrossRef] [PubMed]

5. Goncalves, L.M.; Bermudez, V.D.; Ribeiro, H.A.; Mendes, A.M. Dye-sensitized solar cells: A safe bet for the future. *Energy Environ. Sci.* **2008**, *1*, 655–667. [CrossRef]
6. Hardin, B.E.; Snaith, H.J.; McGehee, M.D. The renaissance of dye-sensitized solar cells. *Nat. Photonics* **2012**, *6*, 162–169. [CrossRef]
7. Yella, A.; Lee, H.W.; Tsao, H.N.; Yi, C.Y.; Chandiran, A.K.; Nazeeruddin, M.K.; Diau, E.W.G.; Yeh, C.Y.; Zakeeruddin, S.M.; Grätzel, M. Porphyrin-sensitized solar cells with cobalt (II/III)-based redox electrolyte exceed 12 percent efficiency. *Science* **2011**, *334*, 629–634. [CrossRef] [PubMed]
8. Kakiage, K.; Aoyama, Y.; Yano, T.; Otsuka, T.; Kyomen, T.; Unno, M.; Hanaya, M. An achievement of over 12 percent efficiency in an organic dye-sensitized solar cell. *Chem. Commun.* **2014**, *50*, 6379–6381. [CrossRef] [PubMed]
9. Mathew, S.; Yella, A.; Gao, P.; Humphry-Baker, R.; Curchod, B.F.E.; Ashari-Astani, N.; Tavernelli, I.; Rothlisberger, U.; Nazeeruddin, M.K.; Grätzel, M. Dye-sensitized solar cells with 13% efficiency achieved through the molecular engineering of porphyrin sensitizers. *Nat. Chem.* **2014**, *6*, 242–247. [CrossRef] [PubMed]
10. Ozawa, H.; Okuyama, Y.; Arakawa, H. Dependence of the efficiency improvement of black-dyebased dye-sensitized solar cells on alkyl chain length of quaternary ammonium cations in electrolyte solutions. *ChemPhysChem.* **2014**, *15*, 1201–1206. [CrossRef] [PubMed]
11. Kakiage, K.; Aoyama, Y.; Yano, T.; Oya, K.; Kyomen, T.; Hanaya, M. Fabrication of a high-performance dye-sensitized solar cell with 12.8% conversion efficiency using organic silyl-anchor dyes. *Chem. Commun.* **2015**, *51*, 6315–6317. [CrossRef] [PubMed]
12. Poplavskyy, D.; Nelson, J. Nondispersive hole transport in amorphous films of methoxy-spirofluorene-arylamine organic compound. *J. Appl. Phys.* **2003**, *93*, 341–346. [CrossRef]
13. Bach, U.; Lupo, D.; Comte, P.; Moser, J.E.; Weissortel, F.; Salbeck, J.; Spreitzer, H.; Grätzel, M. Solid-state dye-sensitized mesoporous TiO_2 solar cells with high photon-to-electron conversion efficiencies. *Nature* **1998**, *395*, 583–585.
14. Kruger, J.; Plass, R.; Cevey, L.; Piccirelli, M.; Grätzel, M.; Bach, U. High efficiency solid-state photovoltaic device due to inhibition of interface charge recombination. *Appl. Phys. Lett.* **2001**, *79*, 2085–2087. [CrossRef]
15. Schmidt-Mende, L.; Bach, U.; Humphry-Baker, R.; Horiuchi, T.; Miura, H.; Ito, S.; Uchida, S.; Gratzel, M. Organic dye for highly efficient solid-state dye-sensitized solar cells. *Adv. Mater.* **2005**, *17*, 813–815. [CrossRef]
16. Snaith, H.J.; Moule, A.J.; Klein, C.; Meerholz, K.; Friend, R.H.; Grätzel, M. Efficiency enhancements in solid-state hybrid solar cells via reduced charge recombination and increased light capture. *Nano Lett.* **2007**, *7*, 3372–3376. [CrossRef] [PubMed]
17. Karthikeyan, C.S.; Wietasch, H.; Thelakkat, M. Highly efficient solid-state dye-sensitized TiO_2 solar cells using donor-antenna dyes capable of multistep charge-transfer cascades. *Adv. Mater.* **2007**, *19*, 1091–1095. [CrossRef]
18. Cai, N.; Moon, S.J.; Cevey-Ha, L.; Moehl, T.; Humphry-Baker, R.; Wang, P.; Zakeeruddin, S.M.; Grätzel, M. An organic D-pi-A dye for record efficiency solid-state sensitized heterojunction solar cells. *Nano Lett.* **2011**, *11*, 1452–1456. [CrossRef] [PubMed]
19. Burschka, J.; Dualeh, A.; Kessler, F.; Baranoff, E.; Cevey-Ha, N.L.; Yi, C.Y.; Nazeeruddin, M.K.; Grätzel, M. Tris(2-(1*H*-pyrazol-1-yl)pyridine)cobalt(III) as p-type dopant for organic semiconductors and its application in highly efficient solid-state dye-sensitized solar cells. *J. Am. Chem. Soc.* **2011**, *133*, 18042–18045. [CrossRef] [PubMed]
20. Tan, M.X.; Laibinis, P.E.; Nguyen, S.T.; Kesselman, J.M.; Stanton, C.E.; Lewis, N.S. Principles and applications of semiconductor photoelectrochemistry. *Prog. Inorg. Chem.* **1994**, *41*, 21–144.
21. Hagfeldt, A.; Boschloo, G.; Sun, L.C.; Kloo, L.; Pettersson, H. Dye-sensitized solar cells. *Chem. Rev.* **2010**, *110*, 6595–6663. [CrossRef] [PubMed]
22. Patzke, G.R.; Zhou, Y.; Kontic, R.; Conrad, F. Oxide nanomaterials: Synthetic developments, mechanistic studies, and technological innovations. *Angew. Chem. Int. Ed.* **2011**, *50*, 826–859. [CrossRef] [PubMed]
23. Loh, L.; Dunn, S. Recent progress in ZnO-based nanostructured ceramics in solar cell applications. *J. Nanosci. Nanotechnol.* **2012**, *12*, 8215–8230. [CrossRef] [PubMed]
24. Wali, Q.; Fakharuddin, A.; Jose, R. Tin oxide as a photoanode for dye-sensitised solar cells: Current progress and future challenges. *J. Power Sources* **2015**, *293*, 1039–1052. [CrossRef]

25. Gibson, E.A.; Smeigh, A.L.; Le Pleux, L.; Fortage, J.; Boschloo, G.; Blart, E.; Pellegrin, Y.; Odobel, F.; Hagfeldt, A.; Hammarstrom, L. A p-type NiO-based dye-sensitized solar cell with an open-circuit voltage of 0.35 V. *Angew. Chem. Int. Ed.* **2009**, *48*, 4402–4405. [CrossRef] [PubMed]
26. Odobel, F.; Le Pleux, L.; Pellegrin, Y.; Blart, E. New photovoltaic devices based on the sensitization of p-type semiconductors: Challenges and opportunities. *Acc. Chem. Res.* **2010**, *43*, 1063–1071. [CrossRef] [PubMed]
27. Nattestad, A.; Mozer, A.J.; Fischer, M.K.R.; Cheng, Y.B.; Mishra, A.; Bauerle, P.; Bach, U. Highly efficient photocathodes for dye-sensitized tandem solar cells. *Nat. Mater.* **2010**, *9*, 31–35. [CrossRef] [PubMed]
28. Yang, W.S.; Noh, J.H.; Jeon, N.J.; Kim, Y.C.; Ryu, S.; Seo, J.; Seok, S.I. High-performance photovoltaic perovskite layers fabricated through intramolecular exchange. *Science* **2015**, *348*, 1234–1237. [CrossRef] [PubMed]
29. Kim, H.-S.; Lee, C.-R.; Im, J.-H.; Lee, K.-B.; Moehl, T.; Marchioro, A.; Moon, S.-J.; Humphry-Baker, R.; Yum, J.-H.; Moser, J.E.; *et al.* Lead iodide perovskite sensitized all-solid-state submicron thin film mesoscopic solar cell with efficiency exceeding 9%. *Sci. Rep.* **2012**, *2*. [CrossRef] [PubMed]
30. Yu, Z.; Sun, L. Recent progress on hole-transporting materials for emerging organometal halide perovskite solar cells. *Adv. Energy Mater.* **2015**, *5*. [CrossRef]
31. Salim, T.; Sun, S.; Abe, Y.; Krishna, A.; Grimsdale, A.C.; Lam, Y.M. Perovskite-based solar cells: Impact of morphology and device architecture on device performance. *J. Mater. Chem. A* **2015**, *3*, 8943–8969. [CrossRef]
32. Heo, J.H.; Han, H.J.; Kim, D.; Ahn, T.K.; Im, S.H. Hysteresis-less inverted $CH_3NH_3PbI_3$ planar perovskite hybrid solar cells with 18.1% power conversion efficiency. *Energy Environ. Sci.* **2015**, *8*, 1602–1608. [CrossRef]
33. You, J.; Meng, L.; Song, T.-B.; Guo, T.-F.; Yang, Y.; Chang, W.-H.; Hong, Z.; Chen, H.; Zhou, H.; Chen, Q.; *et al.* Improved air stability of perovskite solar cells via solution-processed metal oxide transport layers. *Nat. Nanotechnol.* **2016**, *11*, 75–81. [CrossRef] [PubMed]
34. Chen, W.; Wu, Y.; Yue, Y.; Liu, J.; Zhang, W.; Yang, X.; Chen, H.; Bi, E.; Ashraful, I.; Grätzel, M.; *et al.* Efficient and stable large-area perovskite solar cells with inorganic charge extraction layers. *Science* **2015**, *350*, 944–948. [CrossRef] [PubMed]
35. Trifiletti, V.; Roiati, V.; Colella, S.; Giannuzzi, R.; De Marco, L.; Rizzo, A.; Manca, M.; Listorti, A.; Gigli, G. NiO/$MAPbI_{3-x}Cl_x$/PCBM: A model case for an improved understanding of inverted mesoscopic solar cells. *ACS Appl. Mater. Interfaces* **2015**, *7*, 4283–4289. [CrossRef] [PubMed]
36. Nejand, B.A.; Ahmadi, V.; Shahverdi, H.R. New physical deposition approach for low cost inorganic hole transport layer in normal architecture of durable perovskite solar cells. *ACS Appl. Mater. Interfaces* **2015**, *7*, 21807–21818. [CrossRef] [PubMed]
37. Li, D.M.; Qin, D.; Deng, M.H.; Luo, Y.H.; Meng, Q.B. Optimization the solid-state electrolytes for dye-sensitized solar cells. *Energy Environ. Sci.* **2009**, *2*, 283–291. [CrossRef]
38. Schmidt-Mende, L.; Gratzel, M. TiO_2 pore-filling and its effect on the efficiency of solid-state dye-sensitized solar cells. *Thin Solid Films* **2006**, *500*, 296–301. [CrossRef]
39. Snaith, H.J.; Schmidt-Mende, L. Advances in liquid-electrolyte and solid-state dye-sensitized solar cells. *Adv. Mater.* **2007**, *19*, 3187–3200. [CrossRef]
40. Ding, I.K.; Tetreault, N.; Brillet, J.; Hardin, B.E.; Smith, E.H.; Rosenthal, S.J.; Sauvage, F.; Gratzel, M.; McGehee, M.D. Pore-filling of spiro-ometad in solid-state dye sensitized solar cells: Quantification, mechanism, and consequences for device performance. *Adv. Funct. Mater.* **2009**, *19*, 2431–2436. [CrossRef]
41. Wu, J.H.; Lan, Z.; Lin, J.M.; Huang, M.L.; Huang, Y.F.; Fan, L.Q.; Luo, G.G. Electrolytes in dye-sensitized solar cells. *Chem. Rev.* **2015**, *115*, 2136–2173. [CrossRef] [PubMed]
42. Smith, D.L.; Saunders, V.I. The structure and polytypism of the beta-modification of copper(I) thiocyanate. *Acta. Crystallogr. B* **1981**, *37*, 1807–1812. [CrossRef]
43. Hehl, R.; Thiele, G. Synthesis and crystal structure of $Me_3NHCu_2(SCN)_3$, $Me_2C = NMe_2Cu_2(SCN)_3$, and $Me_2C = NMe_2Ag_2(SCN)_3$. Three-dimensional networks of thiocyanatometallates(I). *Z. Anorg. Allg. Chem.* **2000**, *626*, 2167–2172. [CrossRef]
44. Nilushi, W.; Thomas, D.A. Copper(I) thiocyanate (CuSCN) as a hole-transport material for large-area opto/electronics. *Semicond. Sci. Technol.* **2015**, *30*, 104002. [CrossRef]
45. O'Regan, B.; Schwartz, D.T. Efficient dye-sensitized charge separation in a wide-band-gap p-n heterojunction. *J. Appl. Phys.* **1996**, *80*, 4749–4754. [CrossRef]

46. Kumara, G.R.R.A.; Konno, A.; Senadeera, G.K.R.; Jayaweera, P.V.V.; De Silva, D.B.R.A.; Tennakone, K. Dye-sensitized solar cell with the hole collector p-CuSCN deposited from a solution in n-propyl sulphide. *Sol. Energy Mater. Sol. Cells* **2001**, *69*, 195–199. [CrossRef]
47. O'regan, B.; Lenzmann, F.; Muis, R.; Wienke, J. A solid-state dye-sensitized solar cell fabricated with pressure-treated P25-TiO_2 and CuSCN: Analysis of pore filling and iv characteristics. *Chem. Mater.* **2002**, *14*, 5023–5029. [CrossRef]
48. O'Regan, B.C.; Lenzmann, F. Charge transport and recombination in a nanoscale interpenetrating network of n-type and p-type semiconductors: Transient photocurrent and photovoltage studies of TiO_2/dye/CuSCN photovoltaic cells. *J. Phys. Chem. B* **2004**, *108*, 4342–4350. [CrossRef]
49. O'Regan, B.C.; Scully, S.; Mayer, A.C.; Palomares, E.; Durrant, J. The effect of Al_2O_3 barrier layers in TiO_2/dye/CuSCN photovoltaic cells explored by recombination and dos characterization using transient photovoltage measurements. *J. Phys. Chem. B* **2005**, *109*, 4616–4623. [CrossRef] [PubMed]
50. Ranasinghe, C.S.K.; Jayaweera, E.N.; Kumara, G.R.A.; Rajapakse, R.M.G.; Onwona-Agyeman, B.; Perera, A.G.U.; Tennakone, K. Tin oxide based dye-sensitized solid-state solar cells: Surface passivation for suppression of recombination. *Mater. Sci. Semicon. Proc.* **2015**, *40*, 890–895. [CrossRef]
51. Perera, V.P.S.; Senevirathna, M.K.I.; Pitigala, P.K.D.D.P.; Tennakone, K. Doping cuscn films for enhancement of conductivity: Application in dye-sensitized solid-state solar cells. *Sol. Energy Mater. Sol. Cells* **2005**, *86*, 443–450. [CrossRef]
52. Premalal, E.V.A.; Kumara, G.R.R.A.; Rajapakse, R.M.G.; Shimomura, M.; Murakami, K.; Konno, A. Tuning chemistry of CuSCN to enhance the performance of TiO_2/N719/CuSCN all-solid-state dye-sensitized solar cell. *Chem. Commun.* **2010**, *46*, 3360–3362. [CrossRef] [PubMed]
53. Premalal, E.V.A.; Dematage, N.; Kumara, G.R.R.A.; Rajapakse, R.M.G.; Shimomura, M.; Murakami, K.; Konno, A. Preparation of structurally modified, conductivity enhanced-p-CuSCN and its application in dye-sensitized solid-state solar cells. *J. Power Sources* **2012**, *203*, 288–296. [CrossRef]
54. Tennakone, K.; Kumara, G.R.R.A.; Kumarasinghe, A.R.; Wijayantha, K.G.U.; Sirimanne, P.M. A dye-sensitized nano-porous solid-state photovoltaic cell. *Semicond. Sci. Technol.* **1995**, *10*, 1689–1693. [CrossRef]
55. Tennakone, K.; Kumara, G.R.R.A.; Kottegoda, I.R.M.; Wijayantha, K.G.U.; Perera, V.P.S. A solid-state photovoltaic cell sensitized with a ruthenium bipyridyl complex. *J. Phys. D Appl. Phys.* **1998**, *31*, 1492–1496. [CrossRef]
56. Kumara, G.R.A.; Konno, A.; Shiratsuchi, K.; Tsukahara, J.; Tennakone, K. Dye-sensitized solid-state solar cells: Use of crystal growth inhibitors for deposition of the hole collector. *Chem. Mater.* **2002**, *14*, 954–955. [CrossRef]
57. Meng, Q.B.; Takahashi, K.; Zhang, X.T.; Sutanto, I.; Rao, T.N.; Sato, O.; Fujishima, A.; Watanabe, H.; Nakamori, T.; Uragami, M. Fabrication of an efficient solid-state dye-sensitized solar cell. *Langmuir* **2003**, *19*, 3572–3574. [CrossRef]
58. Kumara, G.R.A.; Kaneko, S.; Okuya, M.; Tennakone, K. Fabrication of dye-sensitized solar cells using triethylamine hydrothiocyanate as a CuI crystal growth inhibitor. *Langmuir* **2002**, *18*, 10493–10495. [CrossRef]
59. Taguchi, T.; Zhang, X.T.; Sutanto, I.; Tokuhiro, K.; Rao, T.N.; Watanabe, H.; Nakamori, T.; Uragami, M.; Fujishima, A. Improving the performance of solid-state dye-sensitized solar cell using mgo-coated TiO_2 nanoporous film. *Chem. Commun.* **2003**, *9*, 2480–2481. [CrossRef]
60. Kumara, G.R.A.; Okuya, M.; Murakami, K.; Kaneko, S.; Jayaweera, V.V.; Tennakone, K. Dye-sensitized solid-state solar cells made from magnesiumoxide-coated nanocrystalline titanium dioxide films: Enhancement of the efficiency. *J. Photochem. Photobiol. A* **2004**, *164*, 183–185. [CrossRef]
61. Mahrov, B.; Boschloo, G.; Hagfeldt, A.; Siegbahn, H.; Rensmo, H. Photoelectron spectroscopy studies of $Ru(dcbpyH_2)_2(NCS)_2$/CuI and $Ru(dcbpyH_2)_2(NCS)_2$/CuSCN interfaces for solar cell applications. *J. Phys. Chem. B* **2004**, *108*, 11604–11610. [CrossRef]
62. Sakamoto, H.; Igarashi, S.; Niume, K.; Nagai, M. Highly efficient all solid state dye-sensitized solar cells by the specific interaction of CuI with NCS groups. *Org. Electron.* **2011**, *12*, 1247–1252. [CrossRef]
63. Sakamoto, H.; Igarashi, S.; Niume, K.; Nagai, M. All solid state dye-sensitized solar cells by the specific interaction of CuI with NCS groups for practical use. *J. Ceram. Soc. Jpn.* **2012**, *120*, 304–306. [CrossRef]
64. Sakamoto, H.; Igarashi, S.; Uchida, M.; Niume, K.; Nagai, M. Highly efficient all solid state dye-sensitized solar cells by the specific interaction of CuI with NCS groups II. Enhancement of the photovoltaic characteristics. *Org. Electron.* **2012**, *13*, 514–518. [CrossRef]

65. Chung, I.; Lee, B.; He, J.Q.; Chang, R.P.H.; Kanatzidis, M.G. All-solid-state dye-sensitized solar cells with high efficiency. *Nature* **2012**, *485*, 486–489. [CrossRef] [PubMed]
66. Chung, I.; Song, J.H.; Im, J.; Androulakis, J.; Malliakas, C.D.; Li, H.; Freeman, A.J.; Kenney, J.T.; Kanatzidis, M.G. $CsSnI_3$: Semiconductor or metal? High electrical conductivity and strong near-infrared photoluminescence from a single material. High hole mobility and phase-transitions. *J. Am. Chem. Soc.* **2012**, *134*, 8579–8587. [CrossRef] [PubMed]
67. Lee, B.; Stoumpos, C.C.; Zhou, N.J.; Hao, F.; Malliakas, C.; Yeh, C.Y.; Marks, T.J.; Kanatzidis, M.G.; Chang, R.P.H. Air-stable molecular semiconducting lodosalts for solar cell applications: Cs_2Snl_6as a hole conductor. *J. Am. Chem. Soc.* **2014**, *136*, 15379–15385. [CrossRef] [PubMed]
68. He, J.J.; Lindström, H.; Hagfeldt, A.; Lindquist, S.E. Dye-sensitized nanostructured p-type nickel oxide film as a photocathode for a solar cell. *J. Phys. Chem. B* **1999**, *103*, 8940–8943. [CrossRef]
69. Mori, S.; Fukuda, S.; Sumikura, S.; Takeda, Y.; Tamaki, Y.; Suzuki, E.; Abe, T. Charge-transfer processes in dye-sensitized NiO solar cells. *J. Phys. Chem. C* **2008**, *112*, 16134–16139. [CrossRef]
70. Li, L.; Gibson, E.A.; Qin, P.; Boschloo, G.; Gorlov, M.; Hagfeldt, A.; Sun, L.C. Double-layered NiO photocathodes for p-type DSSCs with record IPCE. *Adv. Mater.* **2010**, *22*, 1759–1762. [CrossRef] [PubMed]
71. Qin, P.; Zhu, H.J.; Edvinsson, T.; Boschloo, G.; Hagfeldt, A.; Sun, L.C. Design of an organic chromophore for p-type dye-sensitized solar cells. *J. Am. Chem. Soc.* **2008**, *130*, 8570–8571. [CrossRef] [PubMed]
72. Sumikura, S.; Mori, S.; Shimizu, S.; Usami, H.; Suzuki, E. Syntheses of NiO nanoporous films using nonionic triblock co-polymer templates and their application to photo-cathodes of p-type dye-sensitized solar cells. *J. Photochem. Photobiol. A* **2008**, *199*, 1–7. [CrossRef]
73. Awais, M.; Rahman, M.; MacElroy, J.M.D.; Dini, D.; Vos, J.G.; Dowling, D.P. Application of a novel microwave plasma treatment for the sintering of nickel oxide coatings for use in dye-sensitized solar cells. *Surf. Coat. Technol.* **2011**, *205*, S245–S249. [CrossRef]
74. Powar, S.; Wu, Q.; Weidelener, M.; Nattestad, A.; Hu, Z.; Mishra, A.; Bauerle, P.; Spiccia, L.; Cheng, Y.B.; Bach, U. Improved photocurrents for p-type dye-sensitized solar cells using nano-structured nickel(II) oxide microballs. *Energy Environ. Sci.* **2012**, *5*, 8896–8900. [CrossRef]
75. Zhang, X.L.; Zhang, Z.P.; Huang, F.Z.; Bauerle, P.; Bach, U.; Cheng, Y.B. Charge transport in photocathodes based on the sensitization of NiO nanorods. *J. Mater. Chem.* **2012**, *22*, 7005–7009. [CrossRef]
76. Gibson, E.A.; Awais, M.; Dini, D.; Dowling, D.P.; Pryce, M.T.; Vos, J.G.; Boschloo, G.; Hagfeldt, A. Dye sensitised solar cells with nickel oxide photocathodes prepared via scalable microwave sintering. *Phys. Chem. Chem. Phys.* **2013**, *15*, 2411–2420. [CrossRef] [PubMed]
77. Wood, C.J.; Summers, G.H.; Clark, C.A.; Kaeffer, N.; Braeutigam, M.; Carbone, L.R.; D'Amario, L.; Fan, K.; Farré, Y.; Narbey, S.; *et al.* A comprehensive comparison of dye-sensitized nio photocathodes for solar energy conversion. *Phys. Chem. Chem. Phys.* **2016**, *18*, 10727–10738. [CrossRef] [PubMed]
78. Law, M.; Greene, L.E.; Johnson, J.C.; Saykally, R.; Yang, P.D. Nanowire dye-sensitized solar cells. *Nat. Mater.* **2005**, *4*, 455–459. [CrossRef] [PubMed]
79. Zhang, L.; Boschloo, G.; Hammarstrom, L.; Tian, H. Solid state p-type dye-sensitized solar cells: Concept, experiment and mechanism. *Phys. Chem. Chem. Phys.* **2016**, *18*, 5080–5085. [CrossRef] [PubMed]
80. Fernando, C.A.N.; Kitagawa, A.; Suzuki, M.; Takahashi, K.; Komura, T. Photoelectrochemical properties of rhodamine-C_{18} sensitized p-CuSCN photoelectrochemical cell (PEC). *Sol. Energy Mater. Sol. Cells* **1994**, *33*, 301–315. [CrossRef]
81. Oregan, B.; Schwartz, D.T. Efficient photo-hole injection from adsorbed cyanine dyes into electrodeposited copper(I) thiocyanate thin-films. *Chem. Mater.* **1995**, *7*, 1349–1354. [CrossRef]
82. Sumikura, S.; Mori, S.; Shimizu, S.; Usami, H.; Suzuki, E. Photoelectrochemical characteristics of cells with dyed and undyed nanoporous p-type semiconductor cuo electrodes. *J. Photochem. Photobiol. A* **2008**, *194*, 143–147. [CrossRef]
83. Chitambar, M.; Wang, Z.J.; Liu, Y.M.; Rockett, A.; Maldonado, S. Dye-sensitized photocathodes: Efficient light-stimulated hole injection into p-gap under depletion conditions. *J. Am. Chem. Soc.* **2012**, *134*, 10670–10681. [CrossRef] [PubMed]
84. Kawazoe, H.; Yasukawa, M.; Hyodo, H.; Kurita, M.; Yanagi, H.; Hosono, H. P-type electrical conduction in transparent thin films of $CuAlO_2$. *Nature* **1997**, *389*, 939–942. [CrossRef]
85. Benko, F.A.; Koffyberg, F.P. The optical interband-transitions of the semiconductor $CuGaO_2$. *Phys. Status Solidi A* **1986**, *94*, 231–234. [CrossRef]

86. Yu, M.Z.; Draskovic, T.I.; Wu, Y.Y. Cu(I)-based delafossite compounds as photocathodes in p-type dye-sensitized solar cells. *Phys. Chem. Chem. Phys.* **2014**, *16*, 5026–5033. [CrossRef] [PubMed]
87. Nattestad, A.; Zhang, X.L.; Bach, U.; Cheng, Y.B. Dye-sensitized $CuAlO_2$ photocathodes for tandem solar cell applications. *J. Photonics Energy* **2011**, *1*. [CrossRef]
88. Renaud, A.; Chavillon, B.; Le Pleux, L.; Pellegrin, Y.; Blart, E.; Boujtita, M.; Pauporte, T.; Cario, L.; Jobic, S.; Odobel, F. $CuGaO_2$: A promising alternative for NiO in p-type dye solar cells. *J. Mater. Chem.* **2012**, *22*, 14353–14356. [CrossRef]
89. Ahmed, J.; Blakely, C.K.; Prakash, J.; Bruno, S.R.; Yu, M.Z.; Wu, Y.Y.; Poltavets, V.V. Scalable synthesis of delafossite $CuAlO_2$ nanoparticles for p-type dye-sensitized solar cells applications. *J. Alloy. Compd.* **2014**, *591*, 275–279. [CrossRef]
90. Xu, Z.; Xiong, D.H.; Wang, H.; Zhang, W.J.; Zeng, X.W.; Ming, L.Q.; Chen, W.; Xu, X.B.; Cui, J.; Wang, M.K.; *et al.* Remarkable photocurrent of p-type dye-sensitized solar cell achieved by size controlled $CuGaO_2$ nanoplates. *J. Mater. Chem. A* **2014**, *2*, 2968–2976. [CrossRef]
91. Xu, X.B.; Zhang, B.Y.; Cui, J.; Xiong, D.H.; Shen, Y.; Chen, W.; Sun, L.C.; Cheng, Y.B.; Wang, M.K. Efficient p-type dye-sensitized solar cells based on disulfide/thiolate electrolytes. *Nanoscale* **2013**, *5*, 7963–7969. [CrossRef] [PubMed]
92. Ursu, D.; Vaszilcsin, N.; Banica, R.; Miclau, M. Effect of Al doping on performance of $CuGaO_2$ p-type dye-sensitized solar cells. *J. Mater. Eng. Perform.* **2016**, *25*, 59–63. [CrossRef]
93. Ursu, D.; Miclau, M.; Banica, R.; Vaszilcsin, N. Impact of Fe doping on performances of $CuGaO_2$ p-type dye-sensitized solar cells. *Mater. Lett.* **2015**, *143*, 91–93. [CrossRef]
94. Xiong, D.H.; Zhang, W.J.; Zeng, X.W.; Xu, Z.; Chen, W.; Cui, J.; Wang, M.K.; Sun, L.C.; Cheng, Y.B. Enhanced performance of p-type dye-sensitized solar cells based on ultrasmall Mg-doped $CuCrO_2$ nanocrystals. *ChemSusChem.* **2013**, *6*, 1432–1437. [CrossRef] [PubMed]
95. Renaud, A.; Cario, L.; Deniard, P.; Gautron, E.; Rocquefelte, X.; Pellegrin, Y.; Blart, E.; Odobel, F.; Jobic, S. Impact of Mg doping on performances of $CuGaO_2$ based p-type dye-sensitized solar cells. *J. Phys. Chem. C* **2014**, *118*, 54–59. [CrossRef]
96. Xiong, D.H.; Zhang, Q.Q.; Verma, S.K.; Li, H.; Chen, W.; Zhao, X.J. Use of delafossite oxides $CuCr_{1-x}Ga_xO_2$ nanocrystals in p-type dye-sensitized solar cell. *J. Alloy. Compd.* **2016**, *662*, 374–380. [CrossRef]
97. Yum, J.-H.; Baranoff, E.; Wenger, S.; Nazeeruddin, M.K.; Grätzel, M. Panchromatic engineering for dye-sensitized solar cells. *Energy Environ. Sci.* **2010**, *4*, 842–857. [CrossRef]
98. He, J.; Lindström, H.; Hagfeldt, A.; Lindquist, S.-E. Dye-sensitized nanostructured tandem cell-first demonstrated cell with a dye-sensitized photocathode. *Sol. Energy Mater. Sol. Cells* **2000**, *62*, 265–273. [CrossRef]
99. Nakasa, A.; Suzuki, E.; Usami, H.; Fujimatsu, H. Synthesis of porous nickel oxide nanofiber. *Chem. Lett.* **2005**, *34*, 428–429. [CrossRef]
100. Docampo, P.; Ball, J.M.; Darwich, M.; Eperon, G.E.; Snaith, H.J. Efficient organometal trihalide perovskite planar-heterojunction solar cells on flexible polymer substrates. *Nat. Commun.* **2013**, *4*. [CrossRef] [PubMed]
101. Burschka, J.; Pellet, N.; Moon, S.-J.; Humphry-Baker, R.; Gao, P.; Nazeeruddin, M.K.; Grätzel, M. Sequential deposition as a route to high-performance perovskite-sensitized solar cells. *Nature* **2013**, *499*, 316–319. [CrossRef] [PubMed]
102. Liu, Z.; Zhang, M.; Xu, X.; Bu, L.; Zhang, W.; Li, W.; Zhao, Z.; Wang, M.; Cheng, Y.-B.; He, H. P-type mesoscopic NiO as an active interfacial layer for carbon counter electrode based perovskite solar cells. *Dalton Trans.* **2015**, *44*, 3967–3973. [CrossRef] [PubMed]
103. Liu, Z.; Zhang, M.; Xu, X.; Cai, F.; Yuan, H.; Bu, L.; Li, W.; Zhu, A.; Zhao, Z.; Wang, M.; *et al.* NiO nanosheets as efficient top hole transporters for carbon counter electrode based perovskite solar cells. *J. Mater. Chem.* **2015**, *3*, 24121–24127. [CrossRef]
104. Xu, X.; Liu, Z.; Zuo, Z.; Zhang, M.; Zhao, Z.; Shen, Y.; Zhou, H.; Chen, Q.; Yang, Y.; Wang, M. Hole selective NiO contact for efficient perovskite solar cells with carbon electrode. *Nano Lett.* **2015**, *15*, 2402–2408. [CrossRef] [PubMed]
105. Cao, K.; Zuo, Z.; Cui, J.; Shen, Y.; Moehl, T.; Zakeeruddin, S.M.; Grätzel, M.; Wang, M. Efficient screen printed perovskite solar cells based on mesoscopic TiO_2/Al_2O_3/NiO/carbon architecture. *Nano Energy* **2015**, *17*, 171–179. [CrossRef]

106. Tian, H.; Xu, B.; Chen, H.; Johansson, E.M.J.; Boschloo, G. Solid-state perovskite-sensitized p-type mesoporous nickel oxide solar cells. *ChemSusChem.* **2014**, *7*, 2150–2153. [CrossRef] [PubMed]
107. Wang, K.-C.; Jeng, J.-Y.; Shen, P.-S.; Chang, Y.-C.; Diau, E.W.-G.; Tsai, C.-H.; Chao, T.-Y.; Hsu, H.-C.; Lin, P.-Y.; Chen, P.; *et al.* p-Type mesoscopic nickel oxide/organometallic perovskite heterojunction solar cells. *Sci. Rep.* **2014**, *4*. [CrossRef] [PubMed]
108. Jeng, J.-Y.; Chen, K.-C.; Chiang, T.-Y.; Lin, P.-Y.; Tsai, T.-D.; Chang, Y.-C.; Guo, T.-F.; Chen, P.; Wen, T.-C.; Hsu, Y.-J. Nickel oxide electrode interlayer in $CH_3NH_3PbI_3$ perovskite/pcbm planar-heterojunction hybrid solar cells. *Adv. Mater.* **2014**, *26*, 4107–4113. [CrossRef] [PubMed]
109. Zhu, Z.; Bai, Y.; Zhang, T.; Liu, Z.; Long, X.; Wei, Z.; Wang, Z.; Zhang, L.; Wang, J.; Yan, F.; *et al.* High-performance hole-extraction layer of sol-gel-processed NiO nanocrystals for inverted planar perovskite solar cells. *Angew. Chem. Int. Ed.* **2014**, *53*, 12571–12575.
110. Wang, K.-C.; Shen, P.-S.; Li, M.-H.; Chen, S.; Lin, M.-W.; Chen, P.; Guo, T.-F. Low-temperature sputtered nickel oxide compact thin film as effective electron blocking layer for mesoscopic $NiO/CH_3NH_3PbI_3$ perovskite heterojunction solar cells. *ACS Appl. Mater. Interfaces* **2014**, *6*, 11851–11858. [CrossRef] [PubMed]
111. Chen, W.; Wu, Y.; Liu, J.; Qin, C.; Yang, X.; Islam, A.; Cheng, Y.-B.; Han, L. Hybrid interfacial layer leads to solid performance improvement of inverted perovskite solar cells. *Energy Environ. Sci.* **2015**, *8*, 629–640. [CrossRef]
112. Lai, W.-C.; Lin, K.-W.; Guo, T.-F.; Lee, J. Perovskite-based solar cells with nickel-oxidized nickel oxide hole transfer layer. *IEEE Trans. Electron Dev.* **2015**, *62*, 1590–1595.
113. Lai, W.-C.; Lin, K.-W.; Wang, Y.-T.; Chiang, T.-Y.; Chen, P.; Guo, T.-F. Oxidized Ni/Au transparent electrode in efficient $CH_3NH_3PbI_3$ perovskite/fullerene planar heterojunction hybrid solar cells. *Adv. Mater.* **2016**. [CrossRef]
114. Liu, M.; Johnston, M.B.; Snaith, H.J. Efficient planar heterojunction perovskite solar cells by vapour deposition. *Nature* **2013**, *501*, 395–398. [CrossRef] [PubMed]
115. Subbiah, A.S.; Halder, A.; Ghosh, S.; Mahuli, N.; Hodes, G.; Sarkar, S.K. Inorganic hole conducting layers for perovskite-based solar cells. *J. Phys. Chem. Lett.* **2014**, *5*, 1748–1753. [CrossRef] [PubMed]
116. Hu, L.; Peng, J.; Wang, W.; Xia, Z.; Yuan, J.; Lu, J.; Huang, X.; Ma, W.; Song, H.; Chen, W.; *et al.* Sequential deposition of $CH_3NH_3PbI_3$ on planar nio film for efficient planar perovskite solar cells. *ACS Photonics* **2014**, *1*, 547–553. [CrossRef]
117. Cui, J.; Meng, F.; Zhang, H.; Cao, K.; Yuan, H.; Cheng, Y.; Huang, F.; Wang, M. $CH_3NH_3PbI_3$-based planar solar cells with magnetron-sputtered nickel oxide. *ACS Appl. Mater. Interfaces* **2014**, *6*, 22862–22870. [CrossRef] [PubMed]
118. Park, I.J.; Park, M.A.; Kim, D.H.; Park, G.D.; Kim, B.J.; Son, H.J.; Ko, M.J.; Lee, D.-K.; Park, T.; Shin, H.; *et al.* New hybrid hole extraction layer of perovskite solar cells with a planar p-i-n geometry. *J. Phys. Chem.* **2015**, *119*, 27285–27290. [CrossRef]
119. Xiao, M.; Huang, F.; Huang, W.; Dkhissi, Y.; Zhu, Y.; Etheridge, J.; Gray-Weale, A.; Bach, U.; Cheng, Y.-B.; Spiccia, L. A fast deposition-crystallization procedure for highly efficient lead iodide perovskite thin-film solar cells. *Angew. Chem. Int. Ed.* **2014**, *53*, 9898–9903. [CrossRef] [PubMed]
120. Etgar, L. Hole-transport material-free perovskite-based solar cells. *MRS Bull.* **2015**, *40*, 674–680. [CrossRef]
121. Li, Y.; Ye, S.; Sun, W.; Yan, W.; Li, Y.; Bian, Z.; Liu, Z.; Wang, S.; Huang, C. Hole-conductor-free planar perovskite solar cells with 16.0% efficiency. *J. Mater. Chem. A* **2015**, *3*, 18389–18394. [CrossRef]
122. Kim, J.H.; Liang, P.-W.; Williams, S.T.; Cho, N.; Chueh, C.-C.; Glaz, M.S.; Ginger, D.S.; Jen, A.K.Y. High-performance and environmentally stable planar heterojunction perovskite solar cells based on a solution-processed copper-doped nickel oxide hole-transporting layer. *Adv. Mater.* **2015**, *27*, 695–701. [CrossRef] [PubMed]
123. Jung, J.W.; Chueh, C.-C.; Jen, A.K.Y. A low-temperature, solution-processable, Cu-doped nickel oxide hole-transporting layer via the combustion method for high-performance thin-film perovskite solar cells. *Adv. Mater.* **2015**, *27*, 7874–7880. [CrossRef] [PubMed]
124. Park, J.H.; Seo, J.; Park, S.; Shin, S.S.; Kim, Y.C.; Jeon, N.J.; Shin, H.-W.; Ahn, T.K.; Noh, J.H.; Yoon, S.C.; *et al.* Efficient $CH_3NH_3PbI_3$ perovskite solar cells employing nanostructured p-type NiO electrode formed by a pulsed laser deposition. *Adv. Mater.* **2015**, *27*, 4013–4019. [CrossRef] [PubMed]
125. Yin, X.; Que, M.; Xing, Y.; Que, W. High efficiency hysteresis-less inverted planar heterojunction perovskite solar cells with a solution-derived NiOx hole contact layer. *J. Mater. Chem. A* **2015**, *3*, 24495–24503. [CrossRef]

126. Zhang, H.; Cheng, J.; Lin, F.; He, H.; Mao, J.; Wong, K.S.; Jen, A.K.Y.; Choy, W.C.H. Pinhole-free and surface-nanostructured niox film by room-temperature solution process for high-performance flexible perovskite solar cells with good stability and reproducibility. *ACS Nano* **2016**, *10*, 1503–1511. [CrossRef] [PubMed]
127. Ito, S.; Tanaka, S.; Vahlman, H.; Nishino, H.; Manabe, K.; Lund, P. Carbon-double-bond-free printed solar cells from $TiO_2/CH_3NH_3PbI_3/CuSCN/Au$: Structural control and photoaging effects. *ChemPhysChem.* **2014**, *15*, 1194–1200. [CrossRef] [PubMed]
128. Ito, S.; Tanaka, S.; Manabe, K.; Nishino, H. Effects of surface blocking layer of Sb_2S_3 on nanocrystalline TiO_2 for $CH_3NH_3PbI_3$ perovskite solar cells. *J. Phys. Chem. C* **2014**, *118*, 16995–17000. [CrossRef]
129. Murugadoss, G.; Mizuta, G.; Tanaka, S.; Nishino, H.; Umeyama, T.; Imahori, H.; Ito, S. Double functions of porous TiO_2 electrodes on $CH_3NH_3PbI_3$ perovskite solar cells: Enhancement of perovskite crystal transformation and prohibition of short circuiting. *APL Mater.* **2014**, *2*. [CrossRef]
130. Ito, S.; Tanaka, S.; Nishino, H. Substrate-preheating effects on PbI_2 spin coating for perovskite solar cells via sequential deposition. *Chem. Lett.* **2015**, *44*, 849–851. [CrossRef]
131. Qin, P.; Tanaka, S.; Ito, S.; Tetreault, N.; Manabe, K.; Nishino, H.; Nazeeruddin, M.K.; Grätzel, M. Inorganic hole conductor-based lead halide perovskite solar cells with 12.4% conversion efficiency. *Nat. Commun.* **2014**, *5*, 3834. [CrossRef] [PubMed]
132. Ito, S.; Tanaka, S.; Nishino, H. Lead-halide perovskite solar cells by $CH_3NH_3PbI_3$ dripping on PbI_2-CH_3NH_3I-DMSO precursor layer for planar and porous structures using cuscn hole-transporting material. *J. Phys. Chem. Lett.* **2015**, *6*, 881–886. [CrossRef] [PubMed]
133. Chavhan, S.; Miguel, O.; Grande, H.-J.; Gonzalez-Pedro, V.; Sanchez, R.S.; Barea, E.M.; Mora-Sero, I.; Tena-Zaera, R. Organo-metal halide perovskite-based solar cells with CuSCN as the inorganic hole selective contact. *J. Mater. Chem. A* **2014**, *2*, 12754–12760. [CrossRef]
134. Ma, Y.; Zheng, L.; Chung, Y.-H.; Chu, S.; Xiao, L.; Chen, Z.; Wang, S.; Qu, B.; Gong, Q.; Wu, Z.; *et al.* A highly efficient mesoscopic solar cell based on $CH_3NH_3PbI_{3-x}Cl_x$ fabricated via sequential solution deposition. *Chem. Commun.* **2014**, *50*, 12458–12461. [CrossRef] [PubMed]
135. Ye, S.; Sun, W.; Li, Y.; Yan, W.; Peng, H.; Bian, Z.; Liu, Z.; Huang, C. CuSCN-based inverted planar perovskite solar cell with an average PCE of 15.6%. *Nano Lett.* **2015**, *15*, 3723–3728. [CrossRef] [PubMed]
136. Jung, J.W.; Chueh, C.-C.; Jen, A.K.Y. High-performance semitransparent perovskite solar cells with 10% power conversion efficiency and 25% average visible transmittance based on transparent CuSCN as the hole-transporting material. *Adv. Energy Mater.* **2015**, *5*. [CrossRef]
137. Zhao, K.; Munir, R.; Yan, B.; Yang, Y.; Kim, T.; Amassian, A. Solution-processed inorganic copper(I) thiocyanate (CuSCN) hole transporting layers for efficient p-i-n perovskite solar cells. *J. Mater. Chem. A* **2015**, *3*, 20554–20559. [CrossRef]
138. Christians, J.A.; Fung, R.C.M.; Kamat, P.V. An inorganic hole conductor for organo-lead halide perovskite solar cells. Improved hole conductivity with copper iodide. *J. Am. Chem. Soc.* **2014**, *136*, 758–764. [CrossRef] [PubMed]
139. Huang, F.; Dkhissi, Y.; Huang, W.; Xiao, M.; Benesperi, I.; Rubanov, S.; Zhu, Y.; Lin, X.; Jiang, L.; Zhou, Y.; *et al.* Gas-assisted preparation of lead iodide perovskite films consisting of a monolayer of single crystalline grains for high efficiency planar solar cells. *Nano Energy* **2014**, *10*, 10–18. [CrossRef]
140. Sepalage, G.A.; Meyer, S.; Pascoe, A.; Scully, A.D.; Huang, F.; Bach, U.; Cheng, Y.-B.; Spiccia, L. Copper(I) iodide as hole-conductor in planar perovskite solar cells: Probing the origin of *J-V* hysteresis. *Adv. Funct. Mater.* **2015**, *25*, 5650–5661. [CrossRef]
141. Chen, W.-Y.; Deng, L.-L.; Dai, S.-M.; Wang, X.; Tian, C.-B.; Zhan, X.-X.; Xie, S.-Y.; Huang, R.-B.; Zheng, L.-S. Low-cost solution-processed copper iodide as an alternative to PEDOT:PSS hole transport layer for efficient and stable inverted planar heterojunction perovskite solar cells. *J. Mater. Chem. A* **2015**, *3*, 19353–19359. [CrossRef]
142. Chen, Q.; Zhou, H.; Hong, Z.; Luo, S.; Duan, H.-S.; Wang, H.-H.; Liu, Y.; Li, G.; Yang, Y. Planar heterojunction perovskite solar cells via vapor-assisted solution process. *J. Am. Chem. Soc.* **2014**, *136*, 622–625. [CrossRef] [PubMed]
143. Hossain, M.I.; Alharbi, F.H.; Tabet, N. Copper oxide as inorganic hole transport material for lead halide perovskite based solar cells. *Sol. Energy* **2015**, *120*, 370–380. [CrossRef]

144. Zuo, C.; Ding, L. Solution-processed Cu_2O and CuO as hole transport materials for efficient perovskite solar cells. *Small* **2015**, *11*, 5528–5532. [CrossRef] [PubMed]
145. Chatterjee, S.; Pal, A.J. Introducing Cu_2O thin films as a hole-transport layer in efficient planar perovskite solar cell structures. *J. Phys. Chem. C* **2016**, *120*, 1428–1437. [CrossRef]
146. Wang, Y.; Xia, Z.; Liang, J.; Wang, X.; Liu, Y.; Liu, C.; Zhang, S.; Zhou, H. Towards printed perovskite solar cells with cuprous oxide hole transporting layers: A theoretical design. *Semicond. Sci. Technol.* **2015**, *30*, 054004. [CrossRef]